buildings

Article

Seismic Assessment of Existing Precast Concrete Large-Panel Buildings in Albania: A Case Study

Flogerta Krosi [1], Merita Guri [1] and Svetlana Brzev [2,*]

[1] Department of Architecture and Civil Engineering, Polis University, 1051 Tiranë, Albania; flogerta_krosi@universitetipolis.edu.al (F.K.); merita_guri@universitetipolis.edu.al (M.G.)
[2] Department of Civil Engineering, University of British Columbia, Vancouver, BC V6T 1Z4, Canada
* Correspondence: sbrzev@mail.ubc.ca

Abstract

Precast reinforced concrete (RC) large-panel buildings (LPBs) are a common residential construction typology in urban areas of Eastern European countries, including Albania. Due to the ageing of these buildings, which date back to the 1970s, and the country's high seismic hazard, it is very important to assess their seismic safety. This study presents a code-based seismic assessment of a five-storey case-study building in Tirana, Albania's capital, for which limited information was available and was solely based on the original construction specifications (due to the absence of in situ material testing). A 3D finite-element numerical model was developed using LIRA-SAPR 2024 R2 (version 24.2.0.0) software, and seismic analyses were performed using both multi-modal (response spectra) analysis and the equivalent static analysis procedures according to the current Albanian seismic design code (KTP-N.2-89) and the Eurocode 8 framework (including EN 1998-1 and EN 1998-3). Two different seismic hazard levels were considered to assess the effect of a significantly higher seismic hazard level (compared to the original design) on the seismic safety of older existing LPBs. A demand-to-capacity (DCR) assessment revealed significant structural deficiencies, at both the individual wall-panel level and the wall-assembly level. The representative interior load-bearing wall panel has inadequate flexural and shear capacity, with a DCR of 5.13 for flexure due to a very low vertical reinforcement ratio. The assessment also indicates that the vertical panel joint (D4) is the most critical component of the investigated wall assembly, since its shear capacity is governed by the tensile failure of the steel plate that connects the adjacent wall panels, corresponding to a DCR value of 13.89, indicating very high seismic vulnerability. The seismic assessment of the investigated case-study building may be useful for informing future efforts related to seismic assessment and retrofitting of similar LPBs in Albania and Eastern European countries.

Keywords: precast reinforced concrete construction technology; large-panel buildings; seismic assessment; connections; Albania

Academic Editor: Giuseppina Uva

Received: 8 June 2026
Revised: 17 August 2026
Accepted: 19 August 2026
Published: 25 August 2026

1. Introduction

Large-panel buildings (LPBs) utilise standardized and widely adopted technology for their construction (both residential and public buildings) and were mostly built in the second half of the 20th century to address growing urbanization and housing shortages in the post-WWII period. These buildings constitute a large fraction of the existing urban building stock in Eastern European and Central Asian countries. The main structural elements are precast reinforced concrete (RC) wall and floor panels, which were constructed off-site at a manufacturing plant, subsequently transported to the construction site, and assembled on site. An overview of various large-panel systems in Eastern European countries is presented in UNIDO [1].

Large-scale urban construction of LPBs in urban areas of Albania began in 1972, when a manufacturing plant using Chinese precast construction technology was established in Tirana (Albania's capital) near the existing "Josif Pashko" plant. Precast RC buildings, mostly those with a large panel system, constitute about 5% of the overall building stock in the country [2]. These buildings can be found in large cities like Tirana, Kamëz, Vlorë, Shkodër, Durrës, etc. Albanian LPBs are typically mid-rise residential buildings, usually four to six storeys high. In many cases, these buildings have undergone interventions over time—mainly exterior renovations performed by building inhabitants [3]. The precast building construction practice was discontinued in Albania after the end of the communist regime in 1991, and it was replaced by cast-in-situ RC frame construction.

Due to a long history of damaging earthquakes, the territory of Albania is considered a region of high seismic hazard; this is reflected in the current seismic hazard map of Albania (see Figure 1), which was last updated in 2019 after the 26 November 2019 Durrës earthquake [4], according to the Eurocode 8 requirements. As a result of these seismic hazard revisions, many existing buildings in Albania, including LPBs, are deemed to be unsafe when exposed to design earthquakes with intensities prescribed by the current seismic hazard map.

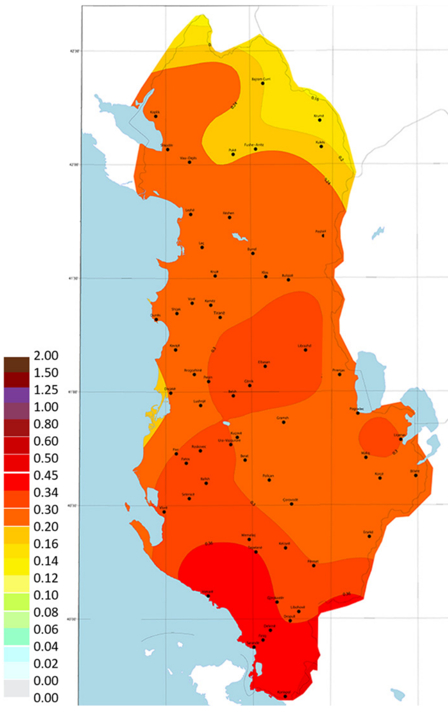

Figure 1. Current seismic hazard map of Albania (issued in 2019) showing reference peak ground accelerations (a_{gR}) according to EN 1998-1:2005 [5] for a 475-year return period design earthquake [4].

The 26 November 2019 Durrës earthquake (Mw 6.4) was the strongest earthquake to hit Albania in the last 40 years, causing 51 deaths and 3000 injuries. It is estimated that 11,490 housing units were severely damaged or collapsed, while an additional 83,745 units experienced damage; this constitutes about 18% of all housing units in 11 affected districts of Albania [6]. Most mid-rise RC framed buildings with masonry infills did not experience structural damage; however, the infills were extensively damaged in many cases. Only a few RC buildings collapsed, mostly due to an irregular configuration (e.g., soft storey irregularity) and acceleration amplification due to soft soil conditions. Low- and mid-rise unreinforced masonry (URM) buildings experienced low to moderate damage, except for a few URM buildings with hollow-core prefabricated RC slabs, which collapsed due to the earthquake and caused casualties.

LPBs generally demonstrated satisfactory seismic performance during the November 2019 Albania earthquake; in the post-earthquake rapid building assessment, 86.2% of the surveyed buildings were assigned a green tag, indicating no structural damage, while only 3.4% were assigned a red tag [6]. A post-earthquake survey conducted by the authors on 834 blocks in LPBs located in Tirana and Durrës after the earthquake showed a limited extent of damage [7]. The results are presented in Figure 2. It can be seen that these buildings experienced minor damage (DG0 or DG1) for seismic intensity up to VII per MMI scale; however, the majority of surveyed buildings experienced DG2 at higher intensities (note that DG0 denotes no damage and DG5 denotes complete destruction, while DG1 and DG2 denote insignificant and minor damage, respectively).

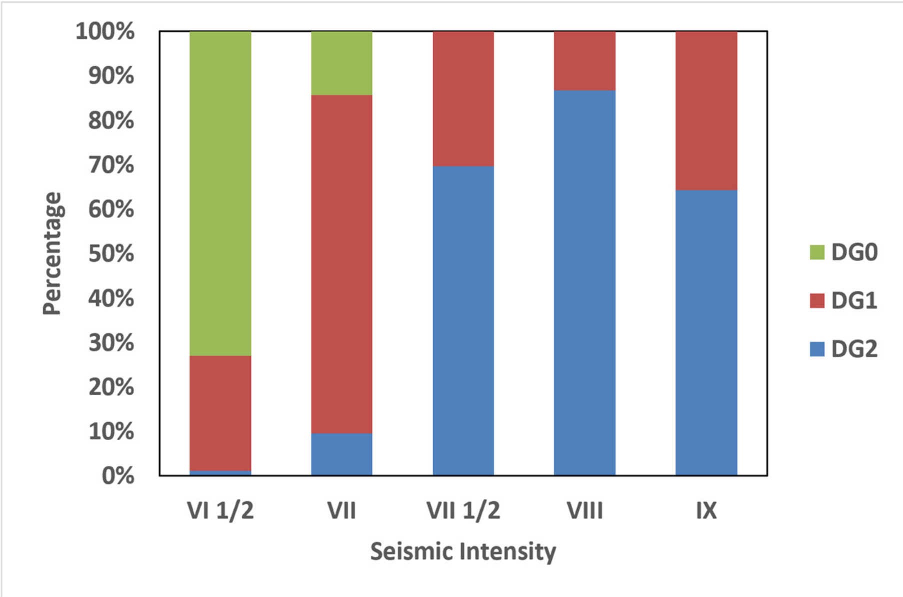

Figure 2. Distribution of observed damage levels in LPBs after the November 2019 Durrës, Albania, earthquake (Mw 6.4) for different seismic intensity levels (MMI scale) in Tirana and Durrës.

The basic structural configuration of LPBs in Albania is a cross-wall system, making them more vulnerable to seismic effects in the longitudinal direction. The observed earthquake damage patterns were in the form of cracking along horizontal and vertical joints [7]. Similar to other existing RC buildings, LPBs are prone to deterioration due to inadequate maintenance and external environmental factors, which may have also contributed to the earthquake damage. Some of the structural interventions observed after the earthquake, such as the creation of new openings in interior wall panels, may have negatively affected the seismic performance of these buildings.

This manuscript presents the first reported study on seismic assessment of a typical Albanian LPB located in the national capital of Tirana. Buildings of this type represent a significant portion of the existing urban building stock in Albania and were exposed to the 2019 Durrës earthquake (Mw 6.4). Although these buildings experienced either minor damage due to the earthquake or remained undamaged altogether, their response to more intense ground shaking is uncertain and needs to be examined.

This study documents, in detail, an Albanian LPB typology through seismic assessment of a case-study building representative of this typology. Structural elements such as precast RC wall and floor panels were constructed in a manufacturing plant based on standardized designs, while the panel connections were assembled and welded on site according to standardized connection details. Although several plan configurations for LPBs have been identified within Albania, they are based on the same structural design concepts, panel typologies, and connection details–the main differences are related to the building length, height, and apartment layout within a building block. Unauthorized structural modifications, material degradation, the effect of local soil conditions, and previous retrofit interventions were not explicitly considered because they vary between individual buildings and are beyond the scope of the present study.

A 3D numerical model of the case-study building was developed by taking into account the geometry of the building and structural elements, as well as the stiffness properties of panel connections, which influenced dynamic properties of the structure. Seismic analyses were performed by applying both an Equivalent Static Analysis (ESA) procedure and Response Spectrum Analysis (RSA) according to the requirements of the current Albanian seismic code (KTP-N.2–89) [8] and the Eurocode seismic design and assessment framework, including Eurocode 8, Part 1 (EC 8-1) [5] and Eurocode 8, Part 3 (EC 8-3) [9]. Different seismic design parameters and seismic hazard levels were taken into account. A lower seismic hazard level was used to reflect the original design and local seismic design code, while a higher seismic hazard level reflects the current national seismic hazard map and Eurocode 8 requirements. The study also features a methodology for seismic assessment of a representative precast RC wall panel and a wall assembly, as well as critical wall-panel connections such as a welded steel-plate vertical joints between the wall panels and a joint along the wall-to-foundation interface.

2. Seismic Behaviour of Existing LPB Systems in Eastern Europe

The main structural elements in LPBs are precast RC horizontal panels (floor structures), vertical panels (wall structures), and their connections. Seismic behaviour and failure mechanisms of LPBs depend on the capacity of the individual panels and their connections, as discussed in this section. The discussion is focused on the existing LPB systems in Eastern Europe.

When subjected to low-intensity earthquakes, LPBs are expected to perform in a manner similar to in situ RC shear walls, without experiencing damage to panels and their connections. A nonlinear response of precast RC wall-panel assemblies, accompanied by significant damage or failure, may occur when the seismic demand (e.g., shear forces or bending moments) is relatively high. In such a case, key structural elements (e.g., wall panels) may experience inelastic deformations (characteristic of ductile assembly behaviour) or a sudden failure (characteristic of brittle assembly behaviour). Alternatively, the connections, usually placed along the vertical and/or horizontal panel joints, may reach their capacity and fail in either a ductile or a brittle manner. Based on the seismic behaviour and failure mechanisms of panel joints (see Figure 3), LPBs can be classified as (i) systems with monolithic behaviour, (ii) systems with weak horizontal joints, or (iii) systems with weak vertical joints [1,7].

Connections and joints in the wall and floor panels have a significant influence on the seismic response and failure mechanisms of LPBs. It should be noted that the panel connections are not standardized across different LPB systems; however, a classification of the connections used in existing large-panel systems in Eastern Europe is currently not available. Depending on the manner in which the panels are connected, the joints may be classified as “wet” or “dry” [1]. Wet joints aim to achieve continuity between the connecting elements to the greatest extent possible. Reinforcing bars are extended from the adjacent panels and are usually lapped, looped, or welded before the concrete is placed in situ to achieve continuity. For example, some of the LPBs in Romania that experienced the

1977 Vrancea earthquake (Mw 7.5) were characterized by wet connections of wall panels and welded horizontal reinforcing bars (see Figure 4a) [1,10,11]. An LPB system in Bulgaria has similar wet connections with welded horizontal reinforcing bars (see Figure 4b) [1].

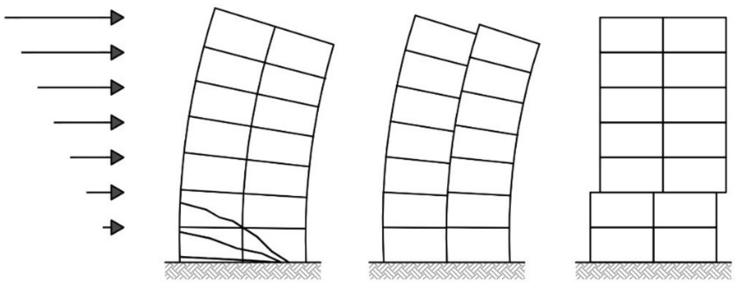

(**a**) (**b**) (**c**)

Figure 3. Seismic failure mechanisms for shear walls in LPBs: (**a**) monolithic behaviour; (**b**) weak vertical joints causing vertical slip; (**c**) weak horizontal joints causing horizontal slip (based on [1]).

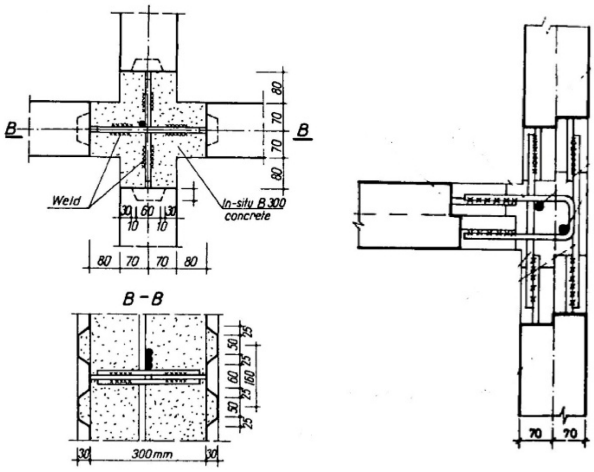

(**a**) (**b**)

Figure 4. Examples of wet connections of wall panels in LPBs: (**a**) a connection of an interior wall panel from Romania; (**b**) a connection of exterior and interior wall panels from Bulgaria. Reproduced from UNIDO [1].

Dry joints are constructed by field welding or bolting of steel plates or other inserts anchored into the adjacent structural elements (e.g., wall panels) and are usually provided at the top/bottom of panels at each floor level (see examples shown in Figure 5a). Therefore, the forces between adjacent elements are transferred at discrete points. Dry joints were used in Albanian LPBs to connect wall panels at the top, as shown in Figure 5b. Note that dry joints in LPBs in Albania were achieved by field welding of steel bars and/or plates, that is, welding was performed at the construction site at the time of building assembly.

The quality of field welding in precast RC buildings may not be satisfactory and could pose a risk of significant damage or failure. For example, poor performance of precast RC frame buildings with welded connections was reported in past earthquakes in the former Soviet Union (e.g., the 1988 Spitak, Armenia earthquake). Brittle failure of welded RC beam and column connections caused fatalities due to building collapses [12,13].

Reports from past earthquakes (e.g., the 1977 Vrancea, Romania, earthquake) indicated that LPBs with wet connections performed in a satisfactory manner and that the connections remained undamaged [10,11]; however, these conclusions are applicable to specific LPB systems and cannot be generalized. Studies on LPBs with dry joints are very limited in the context of existing LPB systems in Eastern Europe.

https://doi.org/10.3390/buildings16173399

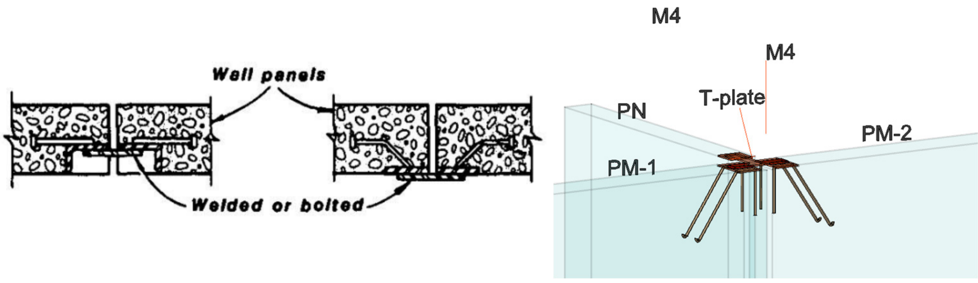

(**a**) (**b**)

Figure 5. Examples of dry wall-panel connections in LPBs: (**a**) wall connections using welded plates with inserts (reproduced from UNIDO [1]) and (**b**) a dry connection of wall panels in the Albanian LPB system considered in this study.

The 1977 Vrancea, Romania, earthquake (Mw 7.5) caused more than 1500 fatalities and severe damage or collapse of a large number of buildings, particularly in Bucharest. At the time of the earthquake, it was estimated that approximately 75,000 apartments in the city were constructed using precast RC large-panel systems [14]. Post-earthquake reconnaissance studies reported that these buildings did not experience significant damage [10]. Several nine-storey precast RC large-panel buildings in Leninakan (Gymri), Armenia, were exposed to the devastating 1988 Spitak earthquake (Mw 6.8), which caused more than 30,000 deaths [13]. These buildings were under construction at the time of the earthquake and did not experience any visible damage. It was reported that a five-storey large-panel building was the only building that remained undamaged in Spitak, the city most affected by the earthquake. Construction technology for RC large-panel buildings reported in Armenia was developed in the Soviet Union and was used throughout the region, as documented in reports from the Russian Federation [15]. The 2012 Pernik, Bulgaria, earthquake (Mw 5.6) caused widespread damage in low- to mid-rise residential and public buildings [16], and the damage was in the form of cracking along horizontal and vertical joints [17]. Many large-panel buildings in Zagreb were exposed to the March 2020 Zagreb, Croatia, earthquake (Mw 5.3); however, these buildings remained undamaged, although many unreinforced masonry buildings experienced damage in the earthquake [18,19].

3. A Review of Past Research Studies on Structural/Seismic Response of LPBs

Experimental and numerical studies on the seismic behaviour and failure mechanisms for LPBs are very limited compared to other structural systems and construction technologies, such as cast in situ RC frame or wall systems.

One of the most comprehensive experimental programmes was conducted on an LPB system, Rad-Balency (originally developed as a French system "Balency"), which was extensively used in the former Yugoslavia [20]. Precast wall panels are connected via wet connections, which consist of horizontal steel reinforcement loops extending from the panels, and vertical reinforcing bars welded at specific locations. The concrete was cast in-situ after the panels were placed in the final position. The experimental studies included cyclic tests on panel connections and three-storey wall-panel assemblies at IZIIS, North Macedonia, as well as shaking table tests of the same wall assemblies [21]. The results indicated satisfactory behaviour of joints under cyclic loading and ductile seismic response of three-storey wall-panel assemblies.

Brzev, Petrovic, and Milicevic [22] studied seismic behaviour of LPBs with vertical shear key joints, including possible failure mechanisms, and compared the capacity predictions for wall-panel assemblies using different code equations and estimates based on research models. The focus was on an LPB system, Jugomont, which was developed and widely used in the former Yugoslavia, and the study used examples from Croatia and Serbia. The authors also reviewed similar systems from a few other countries (Bulgaria, Romania, and Albania) and compared the wall/floor ratio (Wall Index) for typical floor plans available in the literature. The findings indicated that the number of walls in these buildings was relatively low, especially for sites characterised by a moderate to high seismic hazard. Another relevant finding was related to the capacity of wall assembly for the Jugomont system, which was determined by considering various failure mechanisms for the wall panels and the joints. One of the main failure mechanisms for shear key joints was found to be associated with sliding (slip) along the panel joints. Since sliding shear resistance depends on the magnitude of vertical load transferred through a joint, it should not be considered a reliable load-transfer mechanism in structures subjected to seismic actions due to potential eccentricities [23].

Brzev et al. [24] examined the seismic behaviour of LPBs in Albania and Serbia, demonstrating the effect of local soil conditions and soil–structure interaction (SSI) on their seismic response. Kolleger and Bouwkamp [25] performed a numerical study on LPBs to examine the effect of SSI on inter-storey lateral displacements. The results showed that inter-storey displacements due to SSI could be equal to inter-storey displacements caused by seismic forces.

A few numerical models for the simulation of the seismic response of LPBs have been proposed by various researchers. Schricker and Powell [26] performed a numerical study on precast RC large-panel systems, where panels were modelled either as elastic beam-type elements or as 2D FEMs. Joints were modelled as nonlinear spring elements and were able to simulate sliding along the joints and the opening of the joints due to seismic loading. Kianoush, Elmorsi, and Scanlon [27] investigated the seismic response of precast large-panel wall systems, focusing on the roles of coupling beams and horizontal connections. The study demonstrated that systems with deep coupling beams exhibited more stable behaviour than those with slender beams, highlighting the importance of connection detailing and ductility for seismic performance. Pall, Marsh, and Fazio [28] studied the nonlinear dynamic time-history analysis behaviour of RC panel buildings. In the numerical model, interconnected wall panels were treated as elastic cantilevers, and floor diaphragms were rigid. Sanchez, Toranzo, and Nixon [29] developed a 3D nonlinear model of a precast RC building and performed a dynamic analysis using Perform 3D software. The model included precast RC panels and steel connections and was able to simulate both linear and nonlinear material behaviour of concrete and steel. The model also simulated the behaviour of steel connections and SSI. Previous studies have highlighted that the seismic behaviour of precast RC large-panel walls is strongly influenced by the performance of connections, which results in a smaller reduction in ductility compared to cast-in-situ RC structures [30]. Becker, Llorente, and Mueller [31] analytically modelled precast RC panels as linear elastic 'super-elements', with non-linear behaviour concentrated within the connection regions. This approach allowed for the simulation of rocking and sliding, the two primary response mechanisms that define the seismic behaviour of precast RC large-panel walls. Abaev, Valiev, and Kodzaev [32] developed a numerical model for nonlinear seismic analysis of LPBs using the finite-element model (FEM) and LIRA-SAPR software. Bakrysheva and Shashkin [33] investigated the stiffness of horizontal joints in LPBs by comparing analytical formulations according to the methodology developed in the Soviet Union with the results of finite-element analysis. The FEM simulated a wall–floor connection and examined its response to induced displacement of the top wall panel. The results showed that the numerical model and analytical solution give similar values for joint stiffness in the vertical direction (difference of less than 5%); however, the difference is more significant for the joint stiffness in the horizontal direction, particularly for the

https://doi.org/10.3390/buildings16173399

direction perpendicular to the joint. Cordoví et al. [34] studied the seismic behaviour and resistance of precast RC panel structures and their joints by developing a numerical model. Jevtic Rundek et al. [35] performed a numerical study on a precast RC wall-panel assembly, which consisted of two wall panels with vertical shear key joints and rigid beams at the top and bottom. The structural response of the assembly subjected to combined gravity loading and incrementally increasing lateral displacement at the top was simulated by a numerical FEM, and a nonlinear static analysis was performed using Abaqus software.

4. Case-Study Building in Tirana, Albania

4.1. Building Description

The building considered for this study is a five-storey residential building located in the "Kombinat" area of Tirana. The building was constructed in the 1970s at the "Josif Pashko" industrial complex (called Kombinat in Albania) as part of an initiative to build 2000 apartments per year in Tirana by applying an imported (Chinese) technology for the production of precast RC panels. The primary function of these buildings was originally intended to be residential use; however, in recent years, the buildings have been renovated to accommodate additional functions, such as shops and restaurants.

Available information regarding the design and construction of LPBs in Albania, stored in the Central Technical Archive [36], is limited. The original construction drawings, showing floor plans and details of the panel connections, are available; however, there is no information regarding the design of these structures. Furthermore, in situ material testing has not been performed for such buildings; hence, the material properties considered in this study are based on the original construction specifications. Examples of typical LPBs in Tirana, Albania, can be seen in Figure 6b.

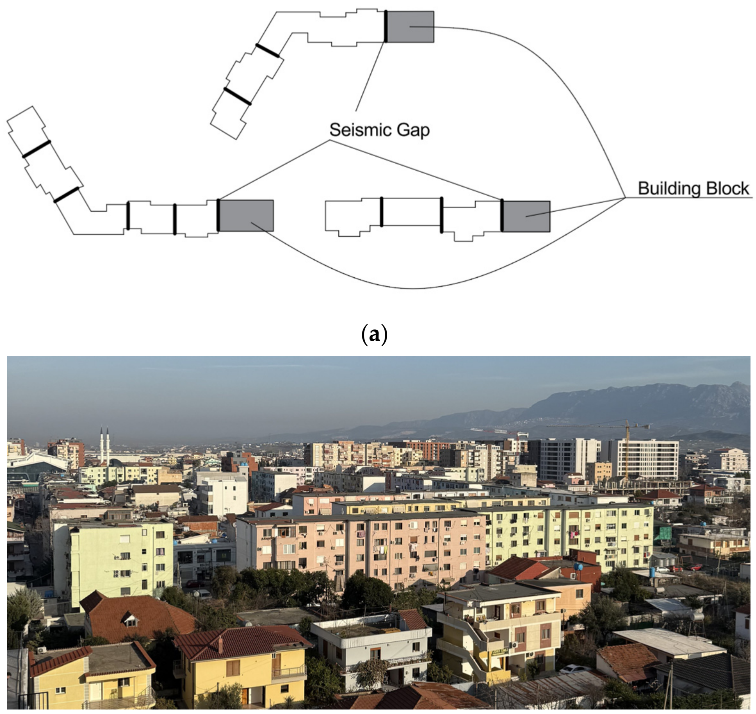

(**a**)

(**b**)

Figure 6. Typical LPBs in Albania: (**a**) examples of building layouts [36] and (**b**) an aerial view of several LPBs in Kamëz (Tiranë).

These buildings usually have an elongated rectangular plan and consist of several building blocks separated by seismic joints, as shown in a typical building plan (see Figure 6a). The floor plan is usually regular, and walls are continuous along the building height. The layout of the walls is mostly uniform in both directions. Figure 7a shows a typical floor plan of an LPB building in Albania. Based on the original construction drawings, it can be concluded that load-bearing walls were provided only in the transverse direction, while only non-load-bearing walls were provided in the longitudinal direction (see Figure 7b). The building is 14.4 m long and 9.9 m wide. The case-study building is five storeys high. The first-storey height is 3.48 m, while each of the upper four storeys has a height of 2.88 m, resulting in a total building height of 15.0 m.

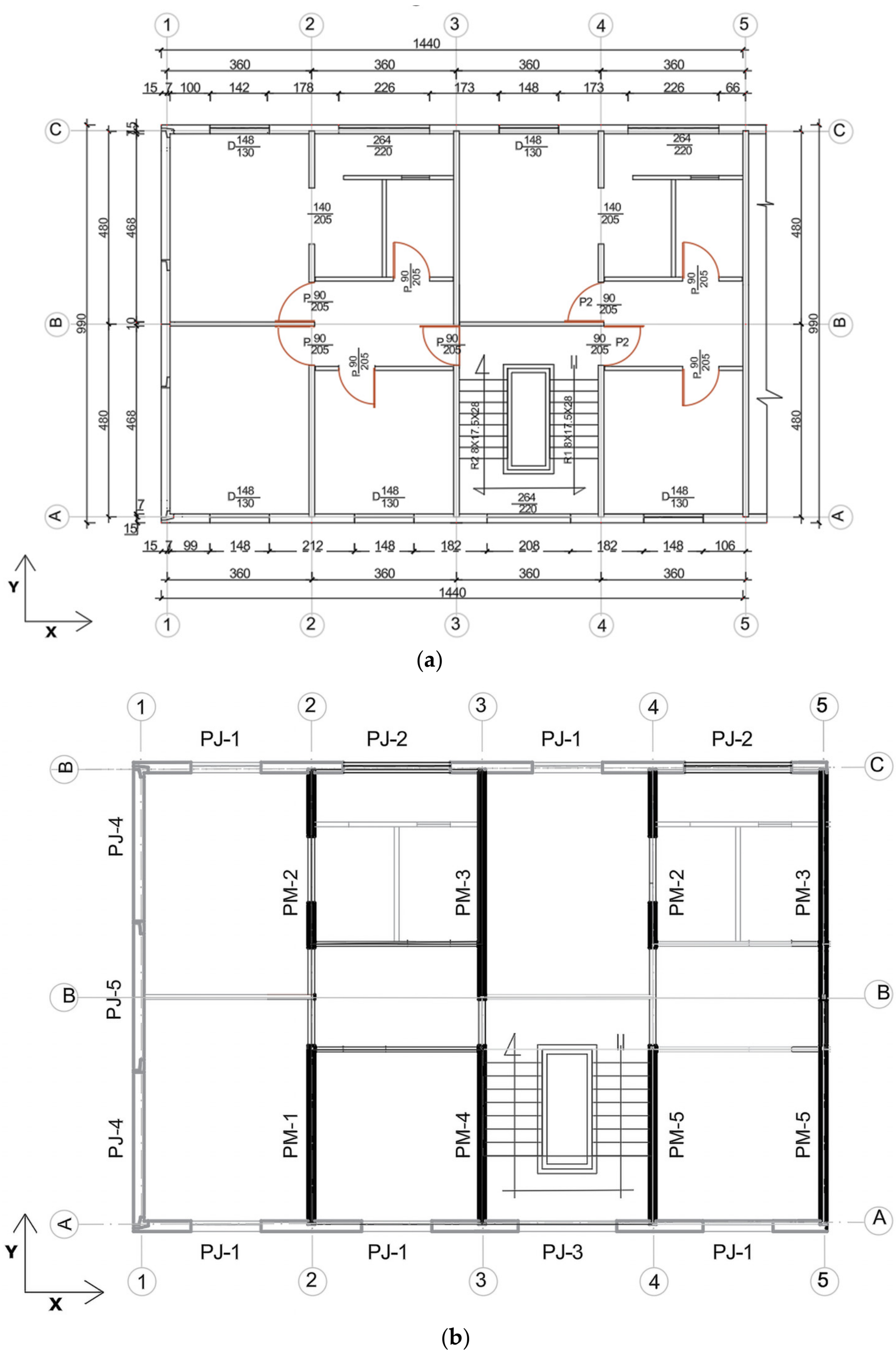

Figure 7. Floor plan for a typical LPB building block: (**a**) architectural plan showing the interior wall layout and (**b**) structural plan with cross-wall system (all dimensions in cm).

Precast large-panel buildings in Albania were constructed using seven distinct types of exterior (façade) wall panels, designated as PJ-1 to PJ-6 (Figure 8a); six interior load-bearing wall panels, labelled as PM-1 to PM-6 (Figure 8b); and six partition (non-load-bearing) wall panels, labelled as PN-1 to PN-6 (Figure 8c). In addition, five different panel types, labelled as S-1 to S-5, were used for the construction of floor slabs.

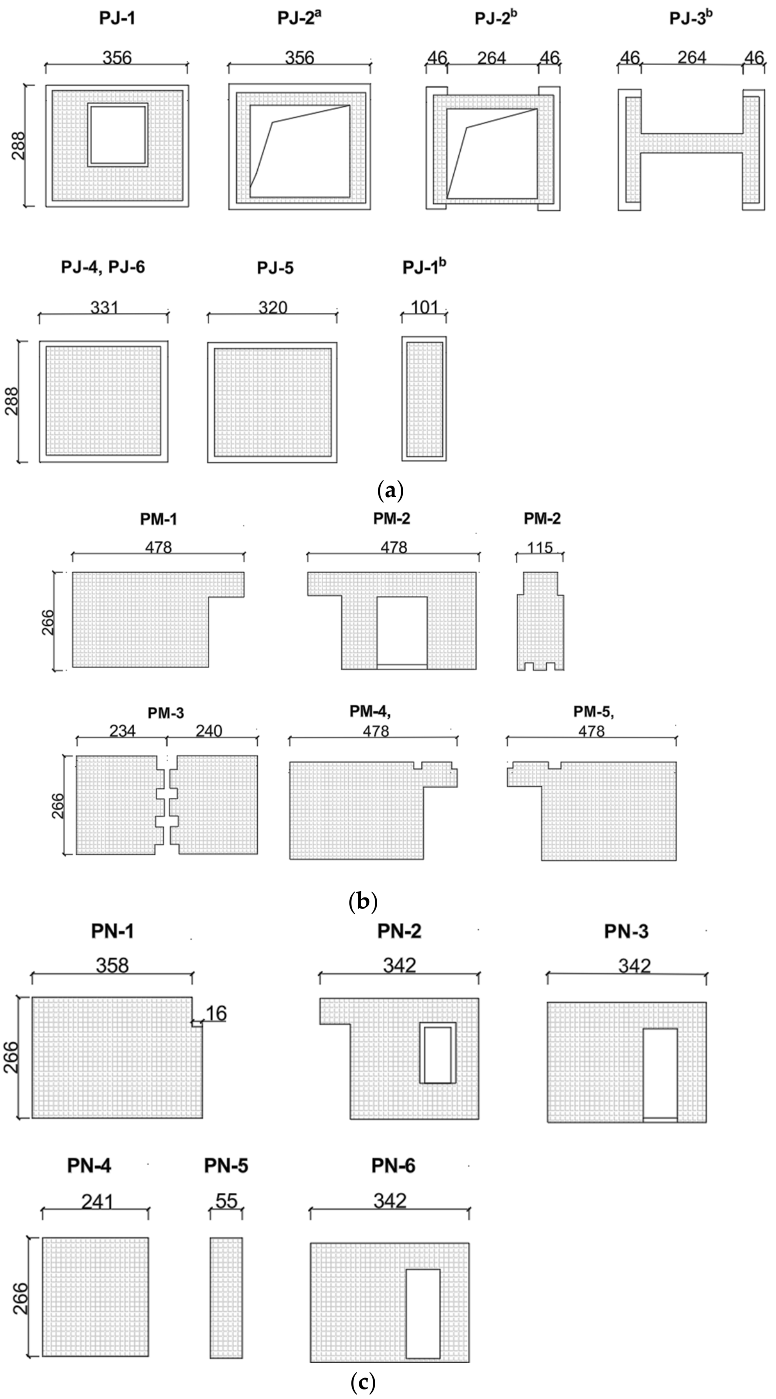

Figure 8. Classification of precast RC wall panels: (**a**) an exterior wall panel (PJ); (**b**) an interior load-bearing wall panel (PM), and (**c**) interior partition wall panels (PN) (all dimensions in cm).

Exterior wall panels (PJ type) are 220 mm thick and consist of 40 mm thick concrete layers at the exterior faces and a 140 mm thick interior polystyrene thermal insulation layer. Note that both lightweight concrete and regular concrete were used for wall construction (see Figure 9a). Load-bearing interior RC panels (PM type) are 140 mm thick, with two steel-mesh reinforcement layers (see Figure 9b). The bar size is Ø4 mm for vertical reinforcement and Ø10 mm for horizontal reinforcement. Additional reinforcement was provided at the wall ends. Detailed information related to wall reinforcement is provided later in this manuscript. The panels were constructed using concrete corresponding to class C16/20 according to the Eurocode 2 classification and steel with $f_{yk} = 340$ MPa.

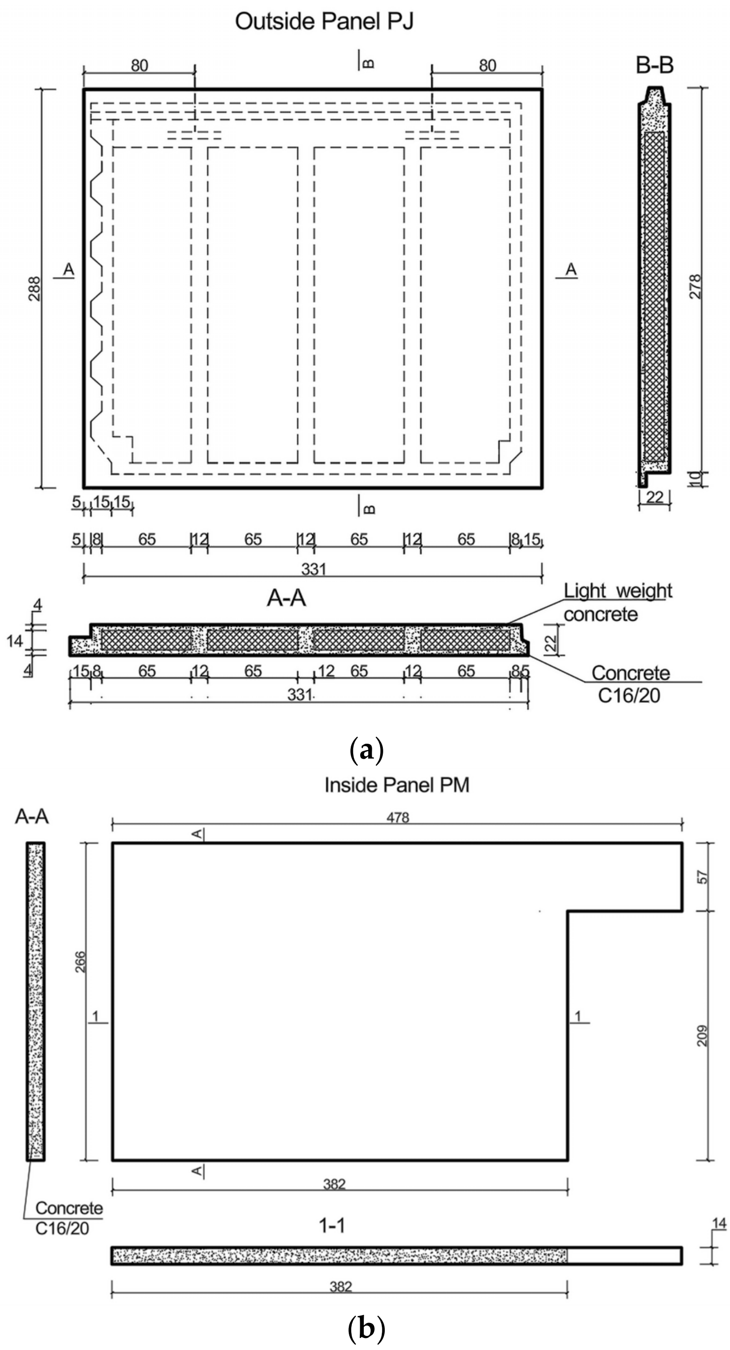

Figure 9. Typical precast RC wall panels in LPBs: (**a**) an exterior non-load-bearing wall panel (PJ type) composed of lightweight concrete and regular concrete and (**b**) an interior load-bearing wall panel (PM type) constructed using regular concrete (all dimensions in cm).

The panels were joined together along horizontal and vertical joints. Different joint types were used, depending on the location. Standardized joints are designated by labels such as D1, D2, D3, and D4 (Figure 10). For example, adjacent load-bearing wall panels (aligned in the transverse direction) are mutually connected at the top via joint D4 (see Figure 11d). It is a dry joint consisting of steel plates with welded anchor bars embedded in each wall panel during the off-site construction stage. During the wall assembly stage at the construction site, another steel plate is welded to connect the embedded plates.

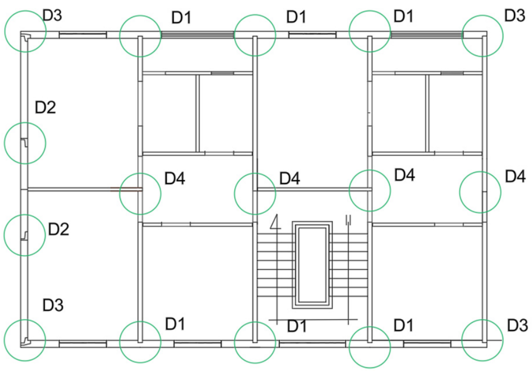

Figure 10. Typical floor plan of an LPB, showing the locations of typical wall panel joints D1, D2, D3, and D4.

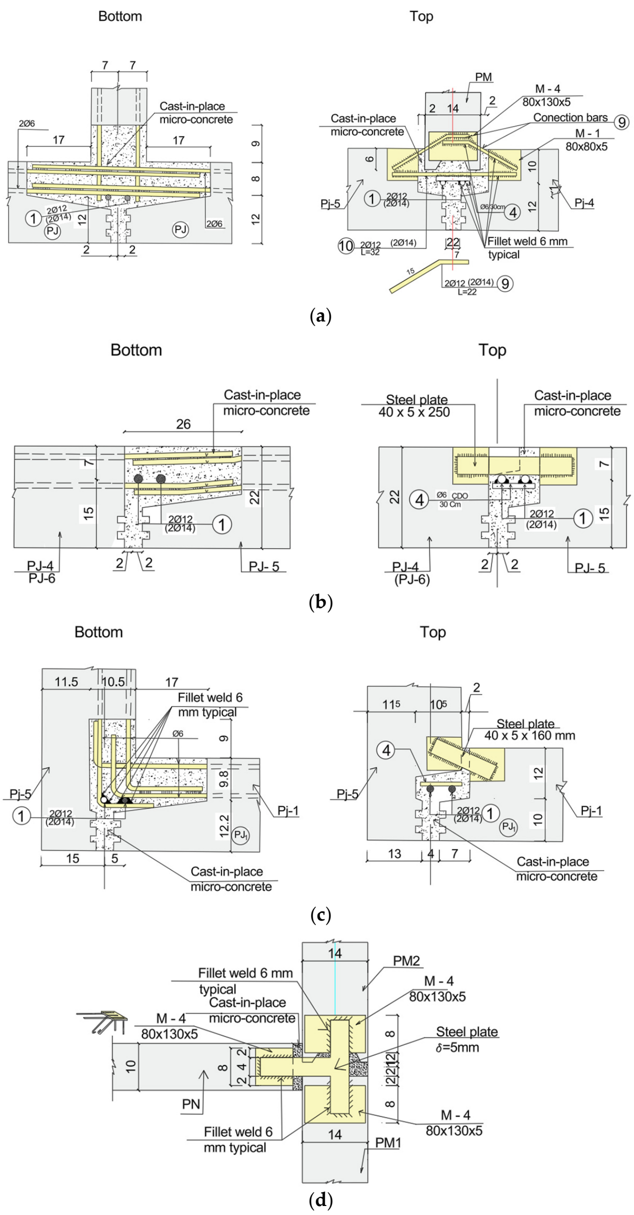

Figure 11. Wall-panel connection details (for top and bottom joints): (**a**) joint D1; (**b**) joint D2; (**c**) joint D3; (**d**) joint D4 (all dimensions in cm).

Although the connection details vary depending on the joint type, they follow the same construction principle. The joint at the base is achieved by lapping horizontal reinforcing bars and placing cast-in-situ concrete (see "Bottom" detail, Figure 11a–c). The joint at the top is achieved via a 5 mm thick steel plate welded to the vertical bars or the connection plate (see "Top" detail, Figure 11). Joints D1 and D2 (Figure 11a,b) are used to connect the exterior and interior panels. Joint D3 (Figure 11c) is a corner joint, connecting exterior panels aligned in the longitudinal and transverse directions.

4.2. Numerical Model of the Case-Study Building

A detailed FEM numerical model of an LPB was developed to perform linear elastic analyses using the LIRA software package. The LIRA-CAD module was used for geometric modelling and definition of the structural model, while the LIRA-SAPR module was used to perform the finite-element analysis. The numerical model, developed using LIRA-SAPR modules, incorporated the stiffness and resistance parameters for panel connections according to Russian codes VSN 32-77 [37] and SP 335.1325800.2017 [38]. Platform joints between the panels were modelled following the methodology presented by Abaev, Valiev, and Kodzaev [39], utilizing specific finite elements (such as FE-59) in the LIRA-SAPR module, which are able to simulate joint stiffness and the complex stress state along the interface between precast RC panels. The wall panels and floor slabs were modelled using FE44 shell finite elements available in the LIRA-SAPR element library, which were able to simulate both the in-plane membrane stresses and flexural stresses due to out-of-plane actions. Note that the wall- and floor-panel stiffness properties were determined based on uncracked (gross) sections.

The numerical model of the building included only the structural components forming the lateral load-resisting system–namely, the transverse wall panels (PM type) shown in Figure 7b, floor slabs, and the corresponding panel connections. The exterior façade panels (PJ type) (see Figure 7b) were taken into account only in terms of their self-weight, which contributed to the total seismic mass of the building. These exterior panels were not treated as structural elements of the lateral load-resisting system because they contain large window openings and consist of sandwich precast elements composed of two thin RC wythes separated by a thermal insulation layer (see Figure 9a).

A 3D finite-element (FE) model was developed in the LIRA-CAD module using 2D shell elements to represent the wall panels, floor slabs, and foundations. A regular FE mesh size of 300 mm was adopted throughout the model.

Boundary conditions were defined by modelling the RC mat foundation using shell FEs supported by distributed elastic soil springs. The elastic foundation was defined by the vertical subgrade reaction coefficient ($C_1 = 29,420$ kN/m^3) and shear interaction coefficient ($C_2 = 19,620$ kN/m). Coefficient C_1 represents the vertical compression stiffness of the supporting soil, whereas C_2 represents the shear interaction between adjacent soil springs.

The seismic masses were in the form of distributed masses due to self-weight and the applied live loads.

Modal responses for the RSA were combined using the Square Root of the Sum of Squares (SRSS) method by considering a sufficient number of modes such that at least 90% of mass participation was achieved as per EC 8-1, Cl. 4.3.3.3.1(3). A modal damping ratio of 5% was adopted, in agreement with the EC 8-1 provisions for seismic analysis of RC structures.

The FE library in the LIRA-CAD module includes link elements, which were specifically developed to simulate the stiffness of panel joints. The horizontal platform joints between wall panels and floor slabs were modelled using the FE59 joint elements (see

Figures 12 and 13). The joint stiffness is determined from the input parameters based on the joint geometry and the material properties. For example, a 20 mm thick M100 cement mortar layer with a characteristic compressive strength of 2.5 MPa was used for the horizontal joints, and the corresponding stress–strain ($\sigma - \varepsilon$) relationship was generated based on the FE59 formulation of the platform joint and was used to determine the equivalent joint stiffness for analysis purposes (Figure 14).

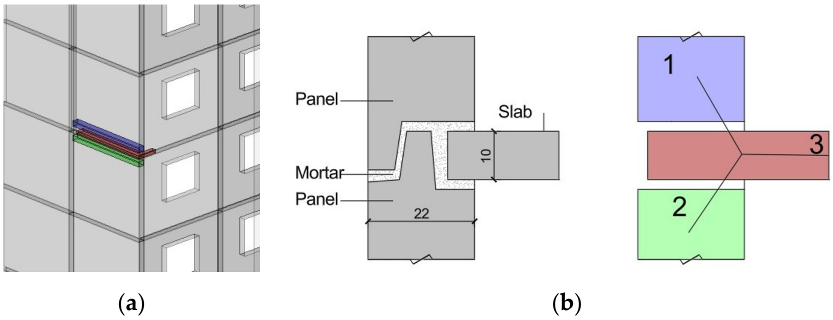

Figure 12. Horizontal joints in the 3D FE numerical model of the building: (**a**) 3D view of the horizontal joint and (**b**) numerical model of the joint FE59 (1 and 2 denote wall panels and 3 denotes slab panel) [40].

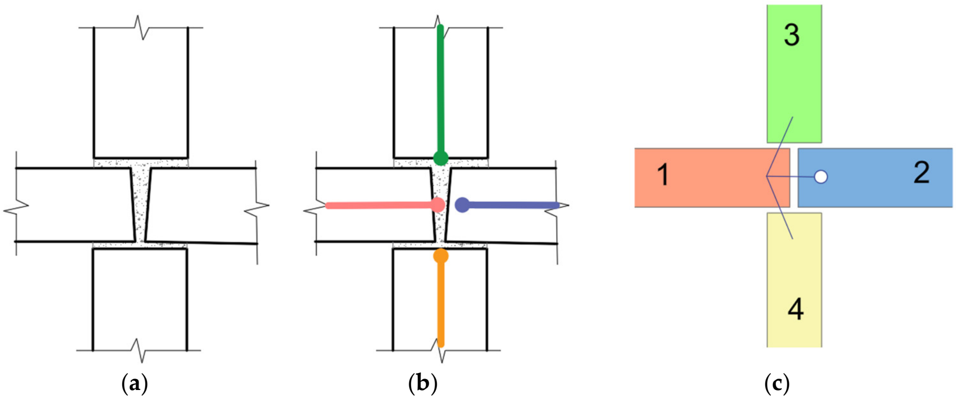

Figure 13. Horizontal joint configuration and geometry: (**a**) geometry of the precast RC wall-panel joint; (**b**) load-transfer directions for joint type FE59; (**c**) conceptual model of the four-panel joint [41].

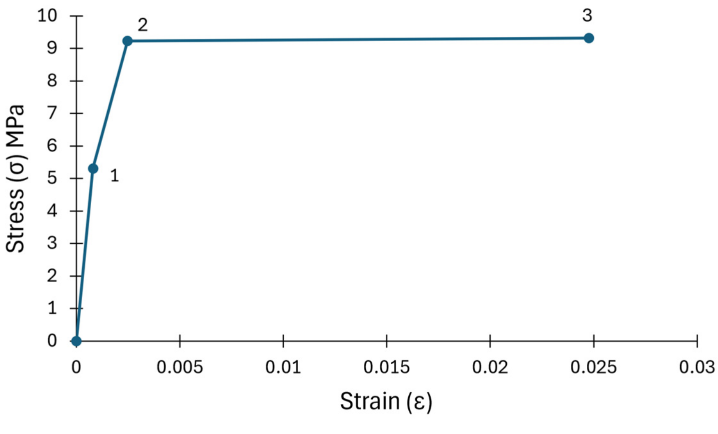

Figure 14. Constitutive stress–strain relation for a horizontal joint generated by the LIRA-CAD module, characterized by the key points 1, 2, and 3 [40].

The panel connections in the horizontal plane were modelled using KE55 linear spring elements, developed to account for the flexibility of connections between structural elements. The stiffness coefficients were first calculated analytically based on the geometry and mechanical properties of the connecting steel components, and the obtained values were assigned to the KE55 elements in the numerical model (see Figure 15). Each KE55 element was defined by two nodes, each having six degrees of freedom defined relative to the axes of the global coordinate system.

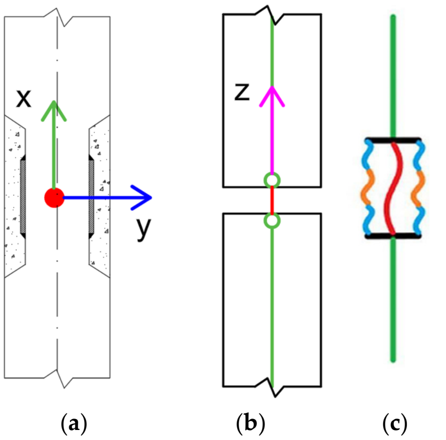

Figure 15. FE model of joint type KE55: (**a**) actual configuration of the joint in horizontal (x-y) plane; (**b**) numerical model of the joint in vertical plane (axis z); (**c**) spring characterizing the joint stiffness [41].

The compliance coefficients along the local x, y, and z axes (see Figure 15) (λ_x, λ_y, and λ_z) are related to the joint flexibility of the welded steel-plate connection. These coefficients were determined according to Equations (1)–(3), considering the geometry of the connections, including their length (l), width (a), thickness (t), and cross-sectional area (A) (see Table 1). Mechanical characteristics of the materials, e.g., steel modulus of elasticity (E = 210 GPa) and shear modulus (G = 84 GPa), were also considered. The corresponding stiffnesses (R_x, R_y, and R_z) were obtained as inverse values of the calculated compliance coefficients from Equations (4)–(6). The calculated compliance and equivalent stiffness values assigned to the KE55 elements for joints D1–D4 are presented in Table 1.

Table 1. Input properties for the panel joints assigned to the KE55 spring elements.

Parameter	D1	D2	D3	D4
Bar diameter (mm)	12			
Plate width (a, mm)		40	40	40
Plate length (l, mm)	40	130	20	50
Plate thickness (t, mm)		5	5	5
Compliance coef. (λ_x, mm/N)	1.68×10^{-6}	3.09×10^{-6}	4.76×10^{-7}	1.19×10^{-6}
Compliance coef. (λ_y, mm/N)	1.06×10^{-7}	2.38×10^{-6}	2.38×10^{-6}	2.38×10^{-6}
Compliance coef. (λ_z, mm/N)	2.49×10^{-5}	0.002	7.62×10^{-6}	0.000119
Stiffness R_x (kN/mm)	593.5	323.1	2100.0	840.0
Stiffness R_y (kN/mm)	9495.4	420.0	420.0	420.0
Stiffness R_z (kN/mm)	40.1	0.5	131.3	8.4

Note that the compliance coefficients (λ_x, λ_y, and λ_z) are expressed in mm/N, whereas the equivalent spring stiffnesses (R_x, R_y, and R_z) are expressed in kN/mm.

$$\lambda_x = \frac{l}{EA} \tag{1}$$

$$\lambda_y = \frac{a}{GA} \tag{2}$$

$$\lambda_z = \frac{l^3}{12EI} \tag{3}$$

$$R_x = \frac{1}{\lambda_x} \quad (4)$$

$$R_y = \frac{1}{\lambda_y} \quad (5)$$

$$R_z = \frac{1}{\lambda_z} \quad (6)$$

4.3. Seismic Design Codes and Analysis Procedures

The main objective of this study was to evaluate the seismic performance of an existing LPB according to both the current Albanian seismic design code (KTP-N.2–89) and the Eurocode 8 framework (including EC 8-1 and EC 8-3). The current Albanian structural design codes, referred to as the Technical Design Conditions [8], were last updated in the late 1980s and were mostly influenced by design standards from the former Soviet Union and Eastern European countries. These regulations do not fully align with contemporary international structural and seismic design codes and do not include a dedicated code for seismic assessment of existing buildings. On the other hand, Eurocodes are also used for design projects in Albania but have not yet been officially adopted, although Council of Ministers' Decree No. 511 issued in 2011 mandated the adoption of Eurocodes for structural and seismic design of buildings. At this time, the implementation of Eurocodes in Albania remains a challenge, but it is believed to represent a crucial step toward improving design and construction, practices [42].

Linear elastic seismic analysis procedures–namely, Equivalent Static Analysis (ESA) and the Response Spectrum Analysis (RSA)–were used in this study. Seismic analysis according to the Albanian seismic design code (KTP-N.2-89) was based on the ESA procedure. The applied seismic forces at each floor level (E_{ki}) are calculated based on Equation (7), as a product of the seismic weight of a building (Q_K); the seismic load distribution coefficient at storey level η_{ki}; and spectral acceleration (S_a), which depends on the fundamental period and the prescribed response spectrum for the building site (see Equation (8)). Seismic weight (Q_K) includes the self-weight of structural elements and a fraction of the live load. The other design parameters that influence the seismic forces include k_E (depends on seismic intensity at the construction site), k_r (depends on the building's importance), Ψ (depends on the structural system and material), and β_i (dynamic coefficient depending on the soil category). The following equation is used to determine seismic forces according to KTP-N.2-89:

$$E_{Ki} = S_a \cdot \eta_{ki} \cdot Q_k \quad (7)$$

where

$$S_a = k_E \cdot k_r \cdot \psi \cdot \beta_i \quad (8)$$

It should be noted that modern seismic design codes consider the effect of the expected ductility of structural elements on the magnitude of seismic forces by including coefficients that depend on the type and material of the structural system and seismic detailing. Note that EC 8-1 prescribes a behaviour factor (q) of 3.0 for the design of new precast RC buildings, while EC 8-3 prescribes a q value of 1.5 for seismic assessment of existing RC buildings (irrespective of the structural system). Both q values (1.5 and 3.0) were used in this study, as discussed in Section 4.4. Although the KTP-N.2-89 code does not prescribe a specific behaviour factor for precast RC buildings, it includes a factor (Ψ) that depends on the structural system and material (as explained above).

The seismic assessment presented in this study is based on the Equivalent Static Analysis (ESA, referred to as the Lateral Force Method of Analysis) according to EC 8-1, Cl. 4.3.3.2. Seismic base shear force (F_b) is determined according to Equation (9). In general, the

ESA procedures prescribed by EC 8-1 and KTP-N.2-89 are similar, except for the difference in elastic response spectra between the two codes. For example, the spectral acceleration ($S_d(T_1)$) according to EC 8-1 is different from the S_a value obtained from the KTP-N.2-89 code. According to EC 8-1, seismic mass (m) includes dead load (self-weight of structural elements) and a fraction of variable (live) load. It should be noted that EC 8-1 also includes a correction factor (λ) that accounts for the effect of higher modes of vibration and is equal to 0.85 for buildings taller than two storeys.

$$F_b = S_d(T_1) \cdot m \cdot \lambda \tag{9}$$

The RSA procedure according to EC 8-1 is based on a design response spectrum for a specific site, which depends on the seismic hazard level, soil type, and modal damping ratio. The shape of the response spectrum depends on the seismic hazard level, with the Type 1 spectrum representing sites with high seismicity, while the Type 2 spectrum is used for lower-seismicity sites. The reference peak ground acceleration on rock (a_{gR}) indicates the expected ground-motion intensity at a particular site. The importance factor (γ_i) accounts for the building's importance, with a value of 1.0 used for structures of regular importance.

The current seismic hazard map of Albania was developed in 2019 by the IGEO [4] (see Figure 1). The map presents peak ground accelerations (PGAs) for various sites corresponding to a design earthquake with a 475-year return period. According to the map, the buildings in Tirana need to be designed for an a_{gR} value of 0.293 g according to EC 8-1. The previous seismic hazard map, used in conjunction with the KTP-N.2-89 code, assigned a peak ground acceleration of 0.12 g for building sites in Tirana.

For this study, the soil class for the building site was classified as "Category C" according to EC 8-1, corresponding to deep layers comprising dense or moderately dense sand, gravel, or stiff clay. According to KTP-N.2-89, the soil was classified as Category II, which includes highly fractured and weathered rock masses; cohesive to moderately cohesive clay–silt deposits; and loose soils such as soft clays, silty clays, sands, and gravels whose consistency depends on moisture conditions.

Figure 16 presents elastic response spectra for Tirana based on the current Albanian seismic design code (KTP-N.2–89) and EC 8-1, which were considered in this study. Note that the KTP-N.2-89 response spectrum corresponds to a PGA value of 0.12 g, while the EC 8-1 response spectra (Type 1) were developed for the a_{gR} values of both 0.12 g and 0.293 g to reflect the seismic hazard levels corresponding to both previous and current hazard maps of Albania.

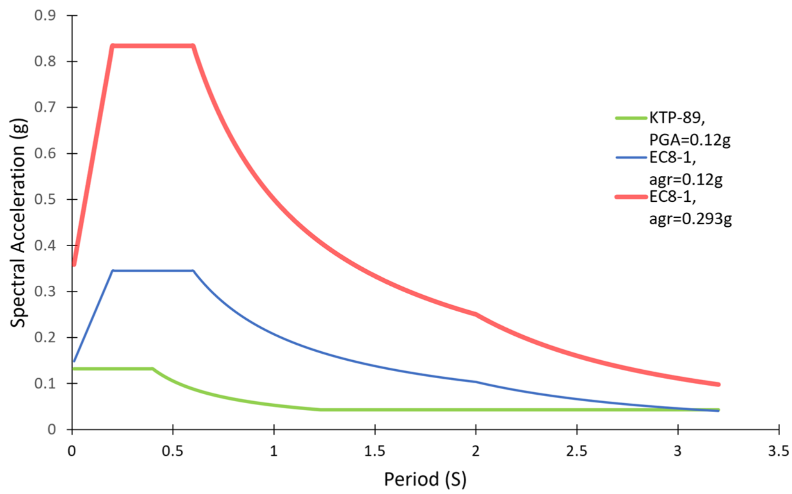

Figure 16. Elastic response spectra for Tirana, Albania, according to the Albanian code (KTP-N.2-89) (0.12 g) and EC 8-1 (considering a_{gR} values of 0.12 g and 0.293 g).

It should be noted that different load combinations are used for the seismic design of buildings according to KTP-N.2-89 and the EC 8-1 (see Equations (10) and (11)). The following load combination is prescribed by KTP-N.2-89:

$$0.9\sum G_t + 0.8\sum P_t + 0.4\sum P + \sum A_{Ed} \quad (10)$$

where G_t is the dead load, P_t is the superimposed permanent load, P is the live load, and A_{Ed} is the seismic load. On the other hand, the load combination according to EC 8-1 is expressed as follows:

$$\sum G_t + 0.3\sum Q_k + \sum A_{Ed} \quad (11)$$

where G_t is the dead load, Q_k is the characteristic value of the imposed (live) load, and A_{Ed} is the seismic load.

4.4. Seismic Assessment Framework

Since the building under consideration is an existing building, seismic assessment should be performed according to EC 8-3, which is a reference code for seismic assessment and retrofitting of existing buildings. The key seismic assessment considerations for the case-study building in the context of EC 8-3 are summarized next.

Knowledge level and confidence factor (Cl. 3.3.1): Since the seismic assessment was performed without in situ material testing, the KL1 knowledge level (limited knowledge) should be assigned. It should be noted that the original construction drawings corresponding to standardized designs were available. These drawings provide information related to the dimensions, reinforcement, and specified material properties for various structural elements. Based on the assigned knowledge level (KL1), the corresponding confidence factor is CF_{KL1}= 1.35.

Material properties (Cl.2.2.1(5) and 3.5.1): EC 8-3 prescribes the use of mean strengths for construction materials (e.g., f_{cm} for concrete), which are larger than the characteristic strengths (e.g., f_{ck} for concrete). These mean strengths were divided by the corresponding confidence-factor (CF) value. For the capacity assessment of brittle primary structural elements, the mean strengths should also be divided by the corresponding partial factor value (Cl.2.2.1(7)); however, unit values of partial factors were used in this study. In addition, considering the age of the investigated building, uncertainties associated with the existing structure may be expected. Existing LPBs may be affected by ageing, reinforcement corrosion, deterioration of mortar, construction deviations, unauthorized interventions, and local damage to panel connections. These factors may influence the mechanical properties and structural behaviour of the building. Since the related information was not available for this study, it is expected that the use of Knowledge Level 1 (KL1) and the related CF value partially account for these uncertainties.

Behaviour factor (q): It is expected that the majority of existing buildings were constructed based on early seismic design codes, which did not contain requirements for ductile design and detailing. For that reason, Cl.2.2.1(4) of EC 8-3 prescribes that a q-factor value of 1.5 be used for all RC structures, irrespective of their structural system. A behaviour factor (q) of 1.5 was used for the ESA in this study; however, a higher behaviour-factor (q) value of 3.0 was considered in the sensitivity analyses and the RSA performed using the LIRA-SAPR module.

Seismic analysis procedure: According to the EN 1998-3 code, nonlinear analysis is not required for the seismic assessment of existing buildings with the assigned knowledge level (KL1). Therefore, the present study adopted linear elastic seismic analysis procedures (ESA and RSA), and the results should be interpreted as a code-based DCR assessment.

Material properties used in this study are summarized in Table 2. Modified mean material strengths for concrete and steel (column 7) were used for the seismic assessment calculations in Section 6. Note that the mean strength values were divided by the CF value and that the unit values of the partial factor were used. A sensitivity analysis was carried out to address various uncertainties related to the material strengths adopted for the case-study building, and the results are summarized in Section 7. Characteristic material strengths according to the EC 8-1 requirements were also used as a reference, reflecting the requirements for new buildings (see column (4)). It can be seen that the modified strength values are lower than the corresponding characteristic values for steel (74.1%) but are higher for concrete (111.1%) (see column (8)).

Table 2. Material properties used for seismic assessment of the case-study building.

Structural Component	Material Designation/Class	Material Property	Characteristic Strength (f_k) (EC 8-1) (MPa)	Mean Strength (EC 8-1) (MPa)	Confidence Factor (*CF*) (EC 8-3)	Modified Mean Strength * $f_m = f_k/CF$ (EC 8-3) (MPa)	f_m/f_k
(1)	**(2)**	**(3)**	**(4)**	**(5)**	**(6)**	**(7) = (5)/(6)**	**(8) = (7)/(4)**
Wall & floor panels	Concrete M200 (KTP) or C16/20 (EC 2)	Concrete-characteristic compressive strength (f_{ck})	16	24	1.35	17.8	111.1%
	Steel (KTP) $R = 3400$ kg/cm^2	Steel reinforcement-characteristic yield strength (f_{yk})	340	340	1.35	251.9	74.1%
Panel connections	Mortar M100 (KTP)	Mortar compressive strength (horizontal joint)	2.5	3.75	1.35	2.8	111.1%
	Concrete C16/20 (EC 2)	Characteristic tensile strength of concrete (f_{ctk})	1.3	1.9	1.35	1.41	108.5%
	Steel (KTP) $R = 2100$ kg/cm^2	Steel plate-characteristic yield strength (f_{yk})	210	210	1.35	155.5	74.1%
	$R^{sal} = 4200$ kg/cm^2	Weld material: tensile strength (f_{uk})	412	412	1.35	305.2	74.1%

Note: * = Unit partial factor values were used to obtain the corresponding mean values.

5. Seismic Analysis: Key Results

5.1. Modal Analysis

Modal analysis results for the 3D FE model developed in the LIRA-SAPR module are presented in Figure 17, showing the first translational and torsional mode shapes. The corresponding fundamental periods of 0.62 s and 0.60 s were obtained for the X and Y directions, respectively. The fundamental period of vibration for the building ($T = 0.38$ s) was estimated based on EC 8-1, Cl.4.3.2.2.2(3) according to the following empirical equation:

$$T = 0.05 \cdot H^{3/4} \tag{12}$$

where H = 15 m is the total building height.

The difference in fundamental periods obtained from the LIRA-SAPR module (0.6 s and 0.62 s) and Equation (12) (0.38 s) is approximately 39%. A smaller fundamental period value obtained from EC 8-1 reflects conservative assumptions regarding the lateral stiffness of RC wall structures. In contrast, the numerical model used for the LIRA-SAPR analyses explicitly accounts for the geometry, material properties, and masses of the case-study building, resulting in a longer fundamental period, which is expected to provide a more realistic representation of its dynamic characteristics.

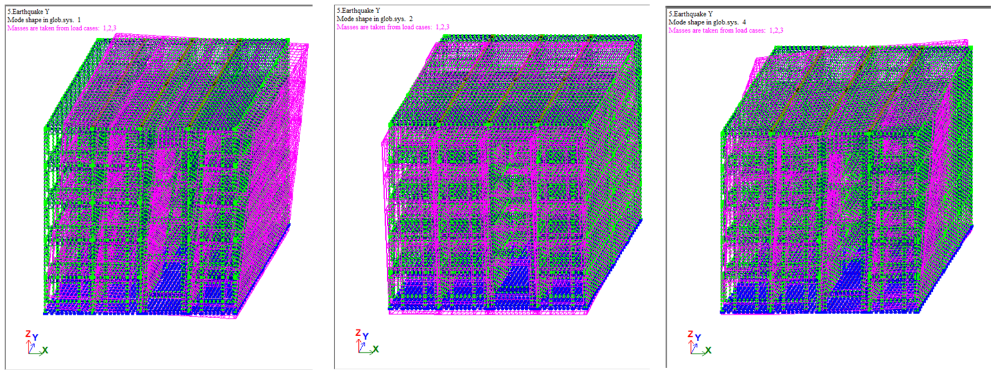

(**a**) (**b**) (**c**)

Figure 17. Mode shapes obtained from the modal analysis of the 3D finite-element model of the case-study building in LIRA-SAPR: (**a**) mode 1 (translational in X direction); (**b**) mode 2 (translational in Y direction); (**c**) mode 4 (torsional).

5.2. Seismic Demand: Shear Forces

In this study, an equivalent static analysis (ESA) of the numerical shear beam model with the masses lumped at the floor levels was performed in accordance with both the current Albanian code (KTP-N.2–89) and Eurocode (the procedure is presented in EC 8-1, but it is referenced by EC 8-3). Subsequently, a response spectrum analysis (RSA) was performed using a 3D numerical model of the building in the LIRA-SAPR module. Figure 18 presents a comparison of seismic shear-force distribution along the building height for the case-study building according to KTP-N.2–89 and Eurocode 8 (EC 8-1 and EC 8-3) for different design ground accelerations (0.12 g and 0.293 g).

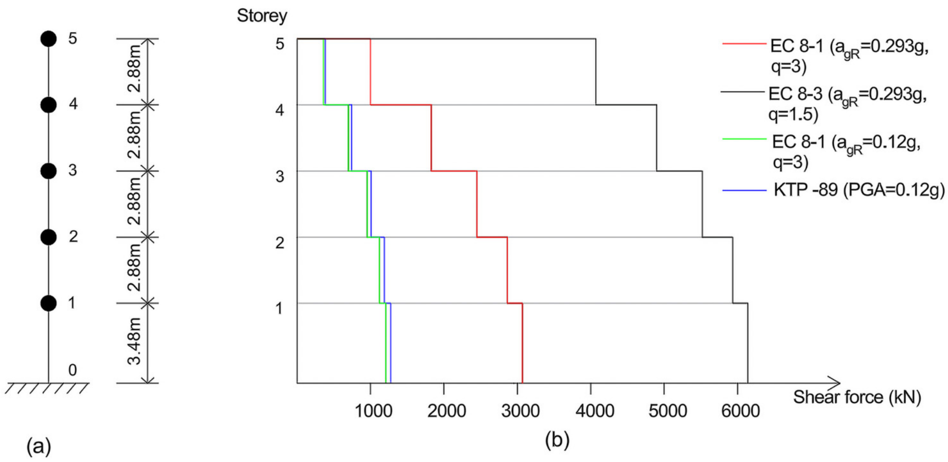

Figure 18. Seismic shear forces for the case study building: (**a**) Shear beam numerical model; (**b**) seismic storey shear-force distribution along the building height according to KTP-N.2–89 and EC 8-1 for different design ground accelerations (0.12 g and 0.293 g).

As a result of the seismic analyses, it was possible to determine the distribution of shear-force demand along the building height, and the results are summarized in Table 3. It should be noted that shear forces obtained from the KTP-N.2–89 code and Eurocode 8 are presented separately.

Table 3. Comparison of seismic storey shear forces obtained from the KTP-N.2–89, EC 8-1, and EC 8-3 codes.

	KTP-N.2-89		EC 8-1		EC 8-1	EC 8-3
Design acceleration	PGA = 0.12 g		a_{gR}= 0.12 g *		a_{gR}= 0.293 g *	a_{gR}= 0.293 g *
Seismic analysis procedure	ESA		ESA		ESA	ESA
Behaviour factor (q)			3.0		3.0	1.5
Floor level	Seismic weight	Storey shear force	Seismic weight	Storey shear force	Storey shear force	Storey shear force
	Q_k (kN)	V (kN)	W_i (kN)	V (kN)	V (kN)	V (kN)
5	2121	382	2136	348	850	1700
4	2483	739	2682	701	1712	3424
3	2483	1007	2682	971	2370	4740
2	2483	1186	2682	1156	2822	5644
1	2483	1276	2682	1257	3070	6140
0		1276		1257	3070	6140
Total	12,053		12,864			

Note: * The seismic action was determined using the EN 1998-1 Type 1 design spectrum for Soil Class C (S = 1.5, $T_B = 0.2$ s, $T_C = 0.6$ s, $T_D = 2$ s) (see Figure 16).

Note that two different seismic hazard levels (expressed in terms of the design acceleration) were considered for seismic analyses. A lower value (a_{gR} = 0.12 g) was used for ESA according to KTP-N.2–89, and the same value $\left(a_{gR} = 0.12 \text{ g}\right)$ was used for ESA according to EC 8-1 in order to compare the results obtained from these two codes. Finally, a higher seismic hazard value $\left(a_{gR} = 0.293 \text{ g}\right)$ was used for the ESA and RSA according to EC 8-1, since that value is in agreement with the latest national seismic hazard map (presented in Figure 1).

The RSA performed in the LIRA-SAPR module using a behaviour factor (q) of 3.0 according to EC 8-1, with $a_{gR} =$ 0.293 g, resulted in a seismic base shear force of 3524 kN. On the other hand, ESA according to EC 8-1 with a behaviour factor (q) of 3.0 resulted in a base shear force of 3070 kN (see Table 3), which is 13% lower than the corresponding force obtained by the RSA performed using LIRA-SAPR. When the design acceleration corresponding to the current KTP-N.2–89 code was used $\left(a_{gR} = 0.12 \text{ g}\right)$, a seismic base shear force of 1276 kN was obtained.

Seismic forces obtained as a result of the ESA according to the EC 8-1 code were significantly higher than those obtained using the KTP-N.2–89 code, primarily due to the higher seismic hazard parameters. The ratio of seismic base shear forces for the EC 8-1 and KTP-N.2–89 codes is 2.32, which closely matches the ratio of the corresponding design acceleration values (0.293 g/0.12 g $\approx$ 2.44). Note that the ESA results for KTP-N.2–89 and EC 8-1 with a behaviour factor (q) of 3.0 for the same design acceleration (0.12 g) are very similar, indicating that the ESA procedures according to these two codes are very similar. As expected, the force demands obtained from the ESA with a behaviour factor (q) of 1.5 are approximately twice those obtained from the ESA with a behaviour factor (q) of 3, reflecting a significantly higher seismic demand for structures with limited ductility. It should be noted that the seismic assessment in this study was performed for a q of 1.5, in accordance with the EC 8-3 requirements (see last column in Table 3).

After the shear forces were determined at the storey level, these forces were distributed to individual wall panels according the following two approaches: (i) a simplified analytical procedure based on ESA in which the storey shear force was distributed to the individual walls in proportion to their lateral stiffness or (ii) an approach whereby seismic forces in individual wall panels were obtained from the LIRA-SAPR module as a result of the

RSA. The forces reported in Table 4 were obtained from the ESA according to EC 8-3 for a behaviour factor (q) of 1.5 and $a_{gR} = 0.293$ g. The reported values correspond to shear forces in wall panels at different floors (levels 0 to 5; see Figure 18). Gridline numbers identify the locations of the corresponding wall panels (PM-1 to PM-5) on the floor plan (see Figure 7a).

Table 4. Seismic forces in wall panels in the Y direction at floor levels (based on the ESA according to EC 8-3 for q = 1.5 and $a_{gR} = 0.293$ g).

		Floor					
Gridline	Panel	5	4	3	2	1	0
		Shear force (kN)					
2	PM-1	120	241	333	397	432	432
	PM-2	79	159	221	263	286	286
3	PM-3	187	377	522	621	676	676
	PM-4	120	241	333	397	432	432
4	PM-2	79	159	221	263	286	286
	PM-5	120	241	333	397	432	432
5	PM-3	187	377	522	621	676	676
	PM-5	120	241	333	397	432	432

In buildings with rigid diaphragms, such as LPBs, seismic shear force at floor level k (V_k) is distributed to individual walls in proportion to their lateral stiffness. Next, the seismic shear force (F_i) acting on an individual wall is calculated as a fraction of the storey shear force (V_k) in proportion to the stiffness of a specific wall (k_i) relative to the stiffness of all walls in the same direction ($\sum K_{\mathrm{i}}$), as follows:

$$F_i = V_k \cdot \frac{K_i}{\sum K_{\mathrm{i}}} \tag{13}$$

The reported shear forces served as the basis for seismic assessment of wall panels. Panel PM-1 along gridline 1 was selected for further assessment because it is a typical panel and is connected to the critical vertical joint (D4), which governs the force transfer between adjacent load-bearing panels (as discussed in the next section). The shear force along the wall section was derived from the shear stress (τ_{xy}) obtained from the numerical model used for RSA in LIRA-SAPR. For each wall panel, the shear force demand was derived by integrating the shear stress distribution over the effective cross-sectional area of the panel (see Figure 19a). The shear force (V) acting on panel PM-1 was derived from the in-plane shear stress distribution (τ_{xy}) obtained from the LIRA-SAPR module by numerically integrating shear stresses over the panel section (A–A) at the base of the wall, as illustrated in Figure 19b, according to Equation (14) as follows:

$$V = \sum A_i \cdot \left(\tau_{xy}\right)_i \tag{14}$$

where $A_i = l_i \times t$ is the tributary cross-sectional area associated with wall segment i, $l_i = 0.31$ m is its tributary length along section A–A, t is the wall thickness, and $\left(\tau_{xy}\right)_i$ is the in-plane shear stress in segment i.

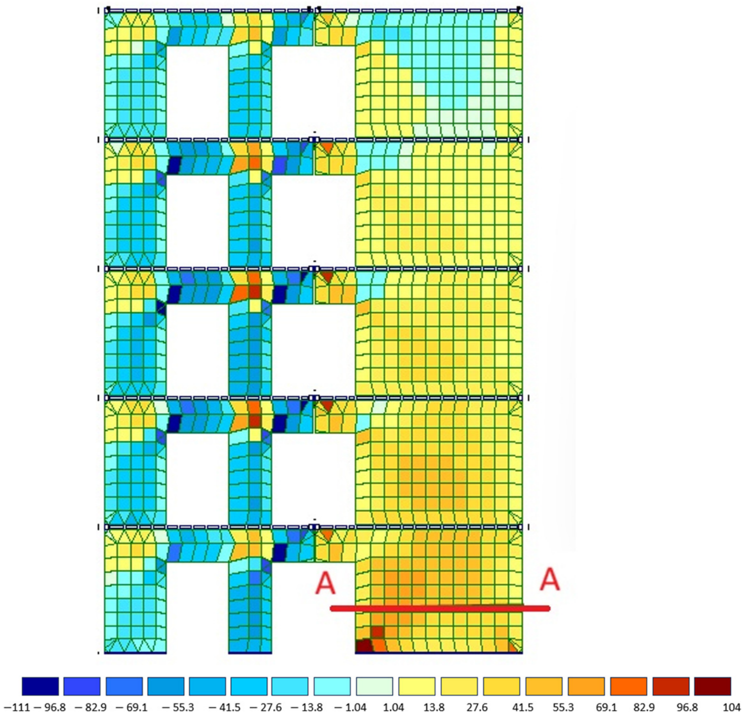

(**a**)

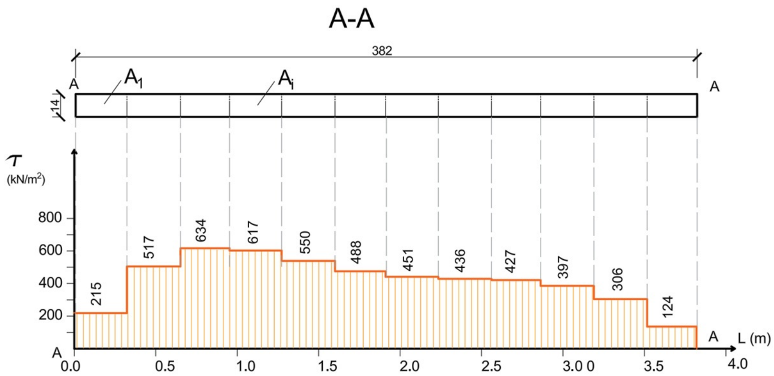

(**b**)

Figure 19. Shear stress distribution in panel PM-1 obtained from the LIRA-SAPR analyses: (**a**) vertical section showing shear stress distribution in panels PM-1 and PM-2 along the building height (units kN/m^2) and (**b**) distribution of shear stress (τ_{xy}) along the wall panel length.

Shear forces obtained from the numerical model represent seismic demand, which was used for the verification of shear resistance of the wall panels and their connections, as discussed in the following sections.

For the critical section at the base of panel PM-1, distribution of seismic force to individual wall panels was determined according to Equation (13), and the resulting shear demand of 216 kN was obtained for panel PM-1 at level 0, with a behaviour factor (q) of 3. Note that the corresponding seismic demand of 432 kN was obtained for q = 1.5 (as shown in Table 4). Alternatively, the resultant shear force was numerically obtained from RSA in the LIRA-SAPR module by integrating the shear stresses distributed over the effective cross-sectional area, as per Equation (14). This procedure resulted in a shear force of 224 kN. The difference between the two values is relatively small (less than 4%, which is satisfactory). It should be noted that the shear demand of 432 kN (see Table 4), corresponding to q = 1.5, was used for seismic assessment according the EC 8-3 code. The seismic assessment of structural elements in this study was based solely on the ESA results, while the RSA results were used to evaluate the global dynamic response of the building and compare it with the ESA results.

5.3. Seismic Displacements

Seismic displacements for the case-study building were obtained from the RSA performed using the LIRA-SAPR module. The displacement envelope in the Y direction is presented in Figure 20a. These displacements were used to calculate the interstorey drifts and the corresponding drift ratios, and the results are summarized in Table 5. It can be seen from the table that the maximum displacement demand at the roof level is 90.1 mm, which corresponds to the seismic displacement induced by the design seismic action according to EC 8-1 Cl.4.3.4. for a behaviour factor (q) of 3.0. It should be noted that the displacement at the base (level 0) of 0.9 mm is attributed to the effect of soil springs that support the mat foundation.

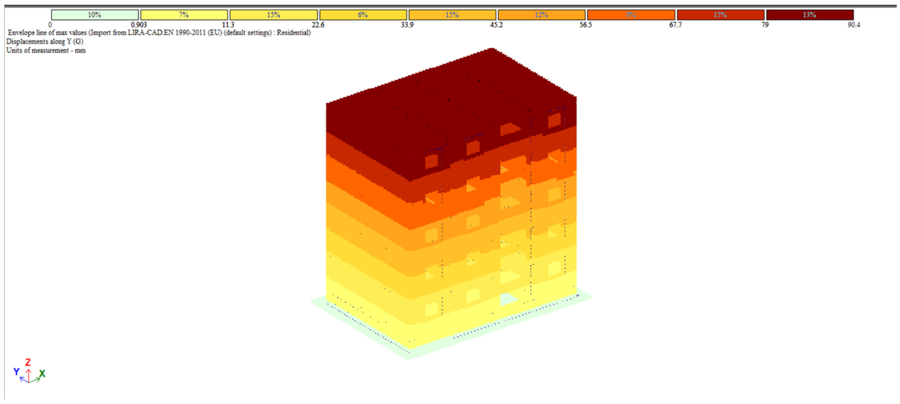

(**a**)

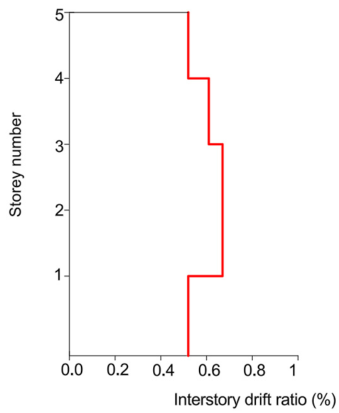

(**b**)

Figure 20. Seismic displacements: (**a**) displacement envelope for the Y direction (LIRA-SAPR) and (**b**) interstorey drift ratio along the building height.

Table 5. Seismic displacements obtained from the RSA using LIRA-SAPR ($a_{gR} = 0.293$ g, $q = 3.0$).

Floor	Lateral Seismic Displacement (mm)	Design Interstorey Drift (mm)	Drift Ratio (%)
5	90.1	14.9	0.52
4	75.2	17.7	0.61
3	57.5	19.2	0.67
2	38.3	19.2	0.67
1	19.1	18.2	0.52
0	0.9		

It should also be noted that the displacements presented in Table 5, calculated using q = 3.0, are significantly lower than the displacements corresponding to q = 1.5, which should be used for seismic assessment according to EC 8-3.

It can be seen from Figure 20b that the drift ratio ranges from 0.52 to 0.67%. Relatively low drift-ratio values could be expected for this building due to the significant amount (number and area) of walls in the Y direction.

According to EC 8-1 Cl. 4.4.3.2, the interstorey drift limit for buildings with non-structural elements constructed using brittle materials attached to the structure is given by

$$d_r \nu \leq 0.005h. \tag{15}$$

The drift-ratio limit can be determined by Equation (15) as follows:

$$\theta_{limit} = \left(\frac{d_r}{h}\right)_{limit} \leq \frac{0.005}{\nu}$$

where d_r is the design interstorey drift; h is the storey height; and ν is the reduction factor associated with the damage limitation state, which depends on the building importance class, in accordance with EC 8-1, Cl. 4.4.3.2(2). Considering a reduction factor of $\nu = 0.5$ for buildings of Importance Class II, the drift-ratio limit can be determined as follows:

$$\theta_{limit}(\%) \leq \frac{0.005}{0.5} = 1.0\%$$

The maximum interstorey drift ratio for this building (0.67%) is less than the EC 8-1 limit of 1.0%, indicating that the seismic displacements are within the acceptable range; however, the drift ratio of 1.34% corresponding to q = 1.5 would exceed the EC 8-1 limit of 1.0%.

In addition to the LIRA-SAPR numerical analysis, the displacement demand for the building was also evaluated in the ESA using the same elastic response spectrum as for the RSA. An approximate estimate of the maximum seismic displacements can be determined based on the relationship between a spectral acceleration (S_a) and the corresponding spectral displacement (S_d) for the given fundamental period (T (s)) of a single-degree-of-freedom (SDOF) system as follows:

$$S_d = \frac{S_a}{\omega^2} \tag{16}$$

where the circular frequency (ω) is

$$\omega = \frac{2\pi}{T} \tag{17}$$

The intersection of the fundamental period ($T = 0.60$ s, from LIRA-SAPR) with the EC 8-1 elastic response spectrum for Tirana ($a_{gR} = 0.293$ g) indicates the spectral acceleration ($S_a = 0.83$ g) (see Figure 16). Consequently, the corresponding elastic spectral displacement with circular frequency calculated according to Equation (17) can be determined by Equation (16) as follows:

$$S_d = \frac{S_a}{\omega^2} = 74\,\text{mm}$$

This displacement is assumed to correspond to the effective building height, where the resulting seismic force is expected to act (provided that only the first vibration mode is considered). The effective height (h_e) is approximately equal to two-thirds of the total building height (h), that is,

$$h_e = \frac{2h}{3} = 10.0\,\text{m}$$

Hence, the maximum elastic displacement at the roof level can be estimated as follows:

$$d_e = S_d \cdot (h/h_e) = 74 \cdot (15.0/10.0) = 111 \text{ mm}$$

It can be concluded that the estimated elastic displacement obtained from the approximate procedure (111 mm) is 23% higher than the maximum displacement obtained from the LIRA-SAPR analysis (90.1 mm) and could be used as a rough estimate for more accurate values obtained in a numerical analysis. It should be noted that the interstorey drift verification performed in this study represents a damage-limitation check according to EC 8-1 and should not be interpreted as evidence of satisfactory life safety performance of the investigated building.

6. Seismic Assessment of Selected Structural Elements

This section presents the methodology for seismic assessment of the case-study building according to the EC 8-3 code requirements and illustrates its application to a typical load-bearing wall panel (PM-1) and a wall assembly consisting of load-bearing wall panels (PM-1 and PM-2). Seismic assessment of these structural elements was performed by determining the corresponding Demand-to-Capacity (DCR) ratios. Seismic demand forces were obtained from the ESA, using a behaviour factor (q) of 1.5 and design acceleration of a_{gR} = 0.293 g. Modified mean values of material properties, as presented in Table 2 (column 7), were used for all calculations presented in this section.

6.1. Seismic Assessment of Wall Panel PM-1

Wall panel PM-1 (see Figure 21) was assessed in terms of DCR according to the EC 8-3 requirements, considering the combined effects of axial force, bending moment, and shear forces. The following design parameters were used for the assessment:

a. Dimensions: length of $l_w = 3.82$ m and thickness of $t = 140$ mm;
b. Material properties: modified mean steel yield strength of $f_{ym} = 251.9$ MPa and modified mean concrete compressive strength of $f_{cm} = 17.8$ MPa (Table 2, column 7);
c. Seismic force demand at the base of the building, obtained from the ESA with a behaviour factor (q) of 1.5 and $a_{gR} = 0.293$ g, as follows:

$$M_{Ed} = 4646 \text{ kNm} \;\; \text{N}_{Ed} = 427 \text{ kN} \;\; V_{Ed} = 432 \;\text{ kN}.$$

6.1.1. Moment Resistance of Wall Panel PM-1 Due to the Combined Effects of Axial Load and Bending

This section evaluates the moment resistance of the wall panel for the combined effects of axial load and bending moment. Moment resistance of the wall section was evaluated using two alternative procedures–the first one produces a simplified closed-form estimate of flexural resistance for RC shear walls with distributed vertical reinforcement, while the second one produces a flexural resistance for an RC shear wall section with distributed and concentrated reinforcement. These procedures are in agreement with the design provisions for RC flexural members presented in EN 1992-1-1:2004 [43] (referred to as EC 2 in this paper) and are explained in the following text.

(a) Moment resistance for an RC shear wall section with distributed vertical reinforcement

In older existing buildings with RC shear walls designed without ductile detailing considerations, vertical reinforcement is usually distributed along the wall length, and there are no boundary elements with concentrated reinforcement. In such a case, the moment resistance can be determined based on an approximate procedure [44], which was adapted for the design of RC shear walls according to the Canadian code for the design of RC structures, CSA A23.3 [45].

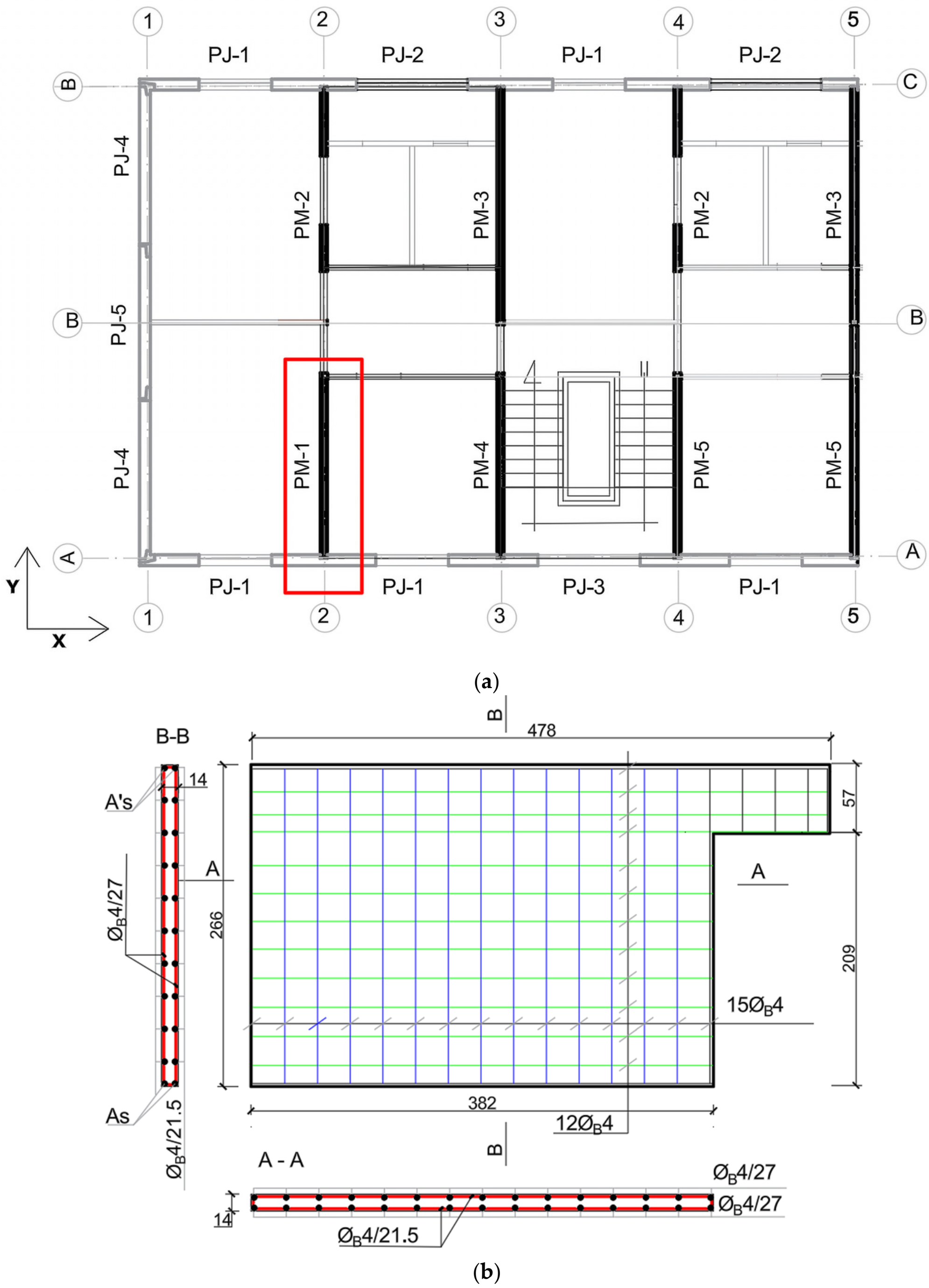

Figure 21. Wall panel PM-1: (**a**) typical floor plan showing the panel location; (**b**) panel dimensions and reinforcement.

The equation for estimating moment resistance for a wall with a length of l and thickness of t was derived based on the assumption that distributed wall reinforcement is treated as an equivalent thin steel plate with a length of l and thickness such that its total area (A_{vt}) is the same as that provided by uniformly distributed reinforcement along the wall length (see Figure 22).

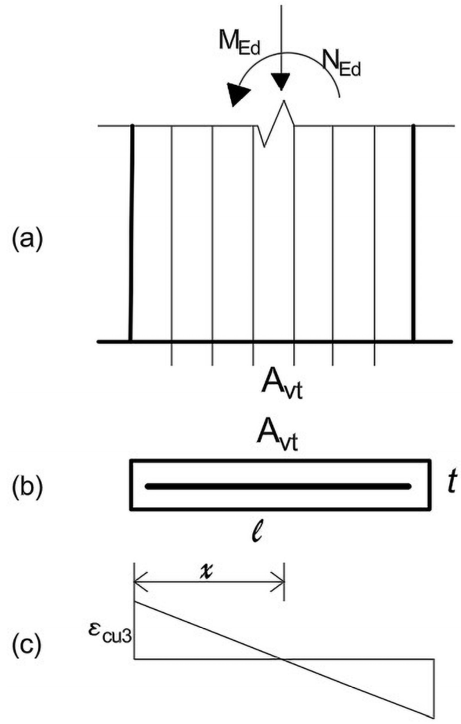

Figure 22. RC shear wall with distributed vertical reinforcement: (**a**) vertical elevation; (**b**) cross-section; (**c**) strain distribution [45].

The equation for determining the moment resistance (M_{Rd}) was adapted to meet the EC 2 requirements as follows:

$$M_{Rd} = 0.5 f_{ym} A_{vt} l \left(1 + \frac{N_{Ed}}{f_{ym} A_{vt}}\right)\left(1 - \frac{x}{l}\right) \quad (18)$$

where x is the neutral axis depth. The ratio of neutral axis depth versus wall length (x/L) was determined according to the following equation:

$$\frac{x}{l} = \frac{\omega + \alpha}{2\omega + \lambda \cdot \eta} \quad (19)$$

where λ = 0.8 and η = 0.567 values correspond to the equivalent rectangular stress-block parameters according to the EC 2 code.

The total area of distributed vertical reinforcement, in the form of two welded reinforcement mesh layers, each containing 15 bars 4 mm in diameter (see Figure 21b), is $A_{vt} = 377\ \mathrm{mm}^2$.

The input parameters for Equation (19) were determined according to

$$\omega = \frac{f_{ym} \cdot A_{vt}}{f_{cm} \cdot l \cdot t} \quad (20)$$

$$\alpha = \frac{N_{Ed}}{f_{cm} \cdot l \cdot t}, \quad (21)$$

and the resulting values are ω =0.01 and $\alpha = 0.045$. Subsequently, an x/L ratio of 0.116 was determined according to Equation (19), taking into consideration Equations (20) and (21); hence, the neutral axis depth is $x = 442$ mm.

Finally, the moment resistance was determined according to Equation (18) as follows:

$$M_{Rd} = 882\ \mathrm{kNm}$$

(b) Moment resistance of RC wall section with distributed and concentrated vertical reinforcement

The flexural resistance of panel PM-1 was obtained as the sum of the moments of the internal force resultants with respect to the centroid (point C) (see Figure 23), as follows:

$$M_{Rd} = F_{cc}\cdot\left(\frac{l}{2} - \frac{0.8x}{2}\right) + F\prime_s\left(\frac{l}{2} - a'\right) + F_s\left(\frac{l}{2} - a\right) \quad (22)$$

where F_{cc} is the resultant compressive force in concrete and F_{sc}, F_s, and F_{sd} represent the resultant forces in the steel reinforcement. Force equilibrium for the wall section can be expressed as follows:

$$N_{ED} = F_{cc} + F_{sc} - F_s \pm F_{sd} \quad (23)$$

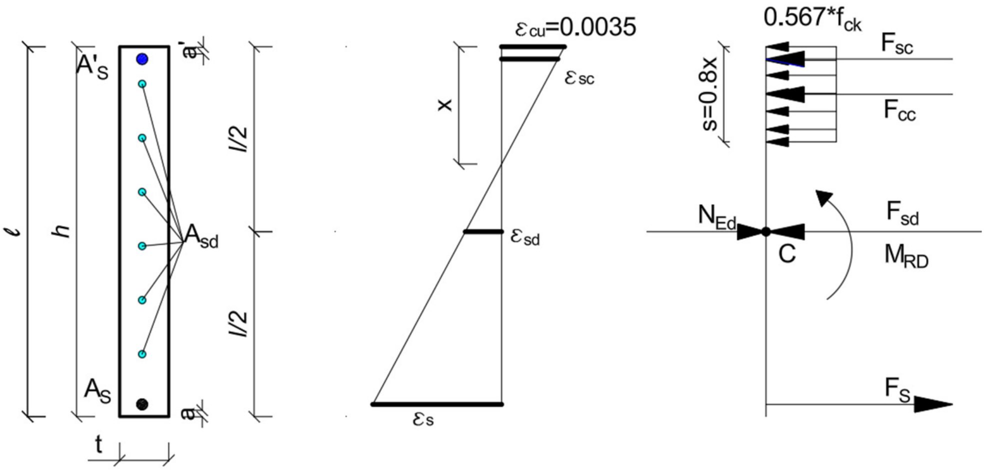

Figure 23. Internal forces and strain distribution for an RC wall section under the combined effects of axial load and bending.

The compressive force in concrete was evaluated using the equivalent rectangular stress block, as per the EC 2 requirements:

$$F_{cc} = 0.567 f_{cm}\cdot t\cdot(0.8x) \quad (24)$$

$$F_{sd} = A_{sd}\cdot f_{sm} \quad (25)$$

$$F_s = A_s\cdot f_{sm} \quad (26)$$

$$F_{sc} = A\prime_s\cdot f_{sm} \quad (27)$$

Note that $f_{sm} = f_{ym}$ when $\varepsilon_s > \varepsilon_y$ and $f_{sm} = E_s\cdot\varepsilon_s$ when $|\varepsilon_s| \le \varepsilon_y$. Wall reinforcement consisted of uniformly distributed vertical reinforcement along the wall length (area A_{sd}) and concentrated reinforcement at wall ends (areas A_s and $A\prime_s$).

Moment resistance (M_{Rd}) for panel PM-1 was determined according to Equation (22). First, the neutral axis depth (x) based on the equilibrium of internal forces, see Equation (23). Subsequently, the strains in steel reinforcement were determined based on the assumption that plane sections remain plane; hence, the strain in distributed, and concentrated steel reinforcement can be determined according to the following relation, considering the maximum compressive strain in concrete ($\varepsilon_{cu3} = 0.0035$):

$$\frac{\varepsilon_{cu3}}{x} = \frac{\varepsilon_s}{l - x - a}$$

The corresponding resultant forces in steel (F_{sc}, F_s, and F_{sd}) were calculated according to Equations (24)–(27). The resultant compression force in concrete was determined according to Equation (24) for a compression-zone depth equal to $0.8x$. Finally, the moment resistance (M_{Rd}) was determined according to Equation (22) as follows:

$$M_{Rd} = 904.77\,\text{kNm}$$

The resulting M_{Rd} values obtained by both approaches (882 kNm and 904.77 kNm) were very similar; the difference is less than 3%.

This assessment also showed that the M_{Rd} value (904.77 kNm) was significantly less than the design bending moment (M_{Ed}) of 4646 kNm; hence, the corresponding DCR value (M_{Ed}/M_{Rd}) is 5.13. A rather low M_{Rd} value can be attributed to a low amount of vertical reinforcement, since the corresponding reinforcement ratio was $\rho_v = 377/(3820{\cdot}140) = 0.071\%$.

6.1.2. Shear Resistance of Wall Panel PM-1

The shear resistance of the wall panel was evaluated according to EC 2, Cl. 6.2.2 and Cl. 6.2.3 by considering the following two cases: (i) shear resistance determined without considering the contribution of shear reinforcement ($V_{Rd,c}$) and (ii) shear resistance determined by taking into account the contribution of the shear reinforcement ($V_{Rd,s}$). The design calculations are presented in this section. Although vertical reinforcement is present in the panel, it is not continuous through the horizontal joint; hence, the longitudinal reinforcement ratio was conservatively disregarded ($\rho = 0$) in the shear resistance calculations.

(a) Shear resistance for an RC wall section without shear reinforcement $(V_{Rd,c})$

The shear resistance of wall panel PM-1 was determined in accordance with EC 2, Cl. 6.2.2 (1) according to the following equation:

$$V_{Rd,c} = \left(v_{\min} + k_1\sigma_{cp}\right)b_w d \tag{28}$$

where the minimum shear strength $v_{\min}$ is

$$v_{\min} = 0.035\,k^{3/2}\,\sqrt{f_{cm}} \tag{29}$$

and a coefficient of $k_1 = 0.15$ was adopted according to EC 2, Cl. 6.2.2. The axial compression stress due to the design axial force ($N_{Ed} = 427\,\text{kN}$) is equal to

$$\sigma_{cp} = \frac{N_{Ed}}{A_c} \tag{30}$$

where the effective cross-sectional wall area is

$$A_c = b_w \cdot d = 534\,800\ \text{mm}^2$$

using $d = 3.82$ m and $b_w = t = 140$ mm; hence, based on Equation (30),

$$\sigma_{cp} = 0.798\ \text{MPa}.$$

The size factor (k) was determined as follows:

$$k = 1 + \sqrt{\frac{200}{d}} = 1.229$$

Finally, the minimum shear strength was determined according to Equation (29) as

$$v_{\min} = 0.201 \text{ MPa},$$

and the corresponding shear resistance of panel PM-1 according to Equation (28) is equal to

$$V_{Rd,c} = 171.6 \text{ kN}.$$

(b) Shear resistance for a wall section with shear reinforcement ($V_{Rd,s}$)

The shear resistance was determined based on EC 2, Cl. 6.2.3. The contribution of horizontal reinforcement, consisting of 2Ø4 bars spaced at s = 215 mm, was determined according to the following equation:

$$V_{Rd,s} = \frac{A_{sw}}{s} \cdot z \cdot f_{ym} \tag{31}$$

where $z = 3438$ mm and $A_{sw} = 25.1$ mm^2 (equal to the area of 2Ø4 bars); hence, based on Equation (31),

$$V_{Rd,s} = 101.6 \text{ kN}.$$

(c) Governing shear resistance

The governing (lower) shear resistance for the wall panel corresponds to a member with shear reinforcement according to EC 2, Cl. 6.2.3; hence, the shear resistance is $V_{Rd} = V_{Rd,s} = 101.6$ kN. This assessment showed that the $V_{Rd,s}$ value is significantly lower than the design shear force ($V_{Rd,s} = 101.6$ kN); hence, the corresponding DCR = 4.25.

6.2. Seismic Assessment of a Wall Assembly Consisting of Panels PM-1 and PM-2 and Their Connections

To perform the seismic assessment of a precast LPB, it is necessary to understand the seismic behaviour of wall assemblies, which comprise two or more adjacent wall panels and their connections. The capacity of an assembly may be governed either by the failure of individual wall panels or by their connections. The governing failure mechanism for a wall assembly is characterized by the lowest capacity. The resistance of individual panels for shear and flexure was discussed in the previous section, while this section presents the seismic assessment approach for a typical wall-panel assembly subjected to shear forces, axial forces, and bending moments due to combined gravity and seismic loads.

A single-storey wall assembly considered in this study consists of panels PM-1 and PM-2, which are aligned along axis 2 (see Figures 24 and 25). The assembly represents a bottom level of a full-height wall assembly in a five-storey building. The panels are connected via vertical joint D4 at the top (Figure 11d) and are supported by the foundations, with horizontal joint J1 provided along the panel-to-foundation interface. It is expected that failure mechanisms for a full-height wall assembly would be similar; however, the failure sequence for the wall panels and their connections at different floor levels would need to be studied. Given the known pattern of seismic force distribution over the building height, it would be expected that the joint damage and failure would initially occur at the lower floor levels.

Connections between the interior structural wall panels (e.g., PM-1 and PM-2) and the façade panels are achieved through welded joints D1 (side joint) and D2 (corner joint) located at the top and bottom of each floor level, respectively (Figure 11a,b).

The shear resistance of a wall assembly subjected to combined gravity and seismic actions was evaluated by considering the following potential failure mechanisms:

1. Flexural failure at the base of the wall assembly (Figure 26a);

2. Simultaneous shear failure of panels PM-1 and PM-2 (Figure 26b);
3. Sliding shear failure along horizontal joint J1 at the base (Figure 26c); and
4. Shear failure of vertical joint D4 (Figure 26d).

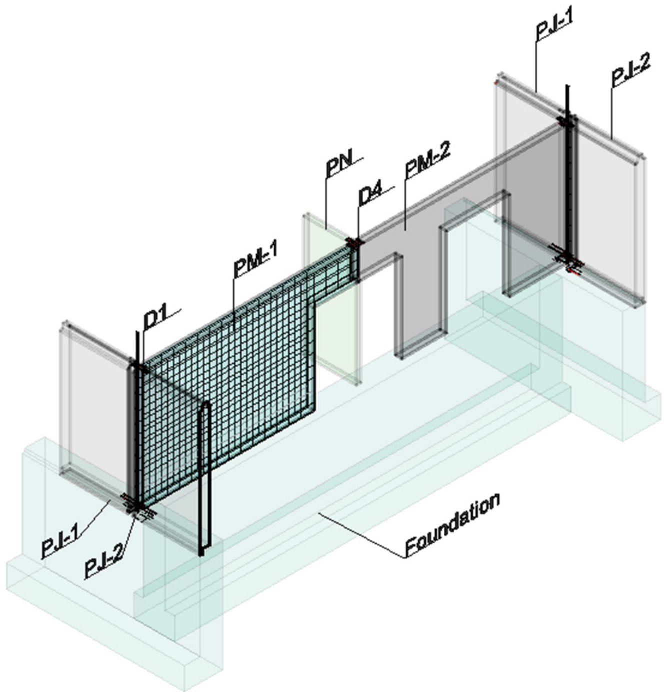

Figure 24. A 3D view of wall panels PM-1 and PM-2, showing the reinforcement detailing, panel connections, and foundation interface.

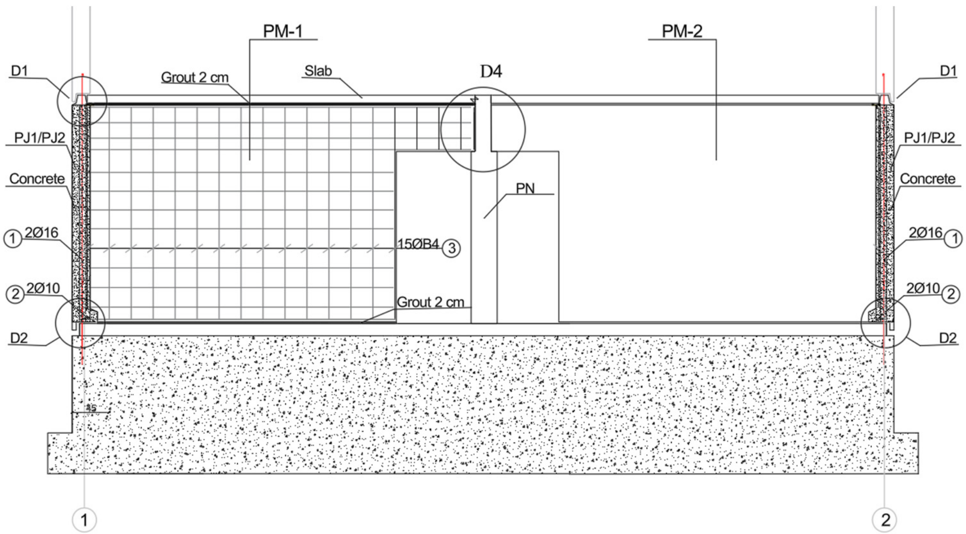

Figure 25. Elevation of precast RC wall panels (PM-1 and PM-2), showing vertical joints, the reinforcement layout, and panel connections.

6.2.1. Shear Force Corresponding to the Flexural Failure of the Wall Assembly

The wall-panel assembly considered in this study consists of two adjacent panels, PM-1 and PM-2, connected through vertical joint D4 through welded steel plates embedded in each panel. Since seismic forces are transferred between the panels through the joint D4, verification is performed for the combined effects of axial force and bending moment acting on the assembly, as illustrated in Figure 27.

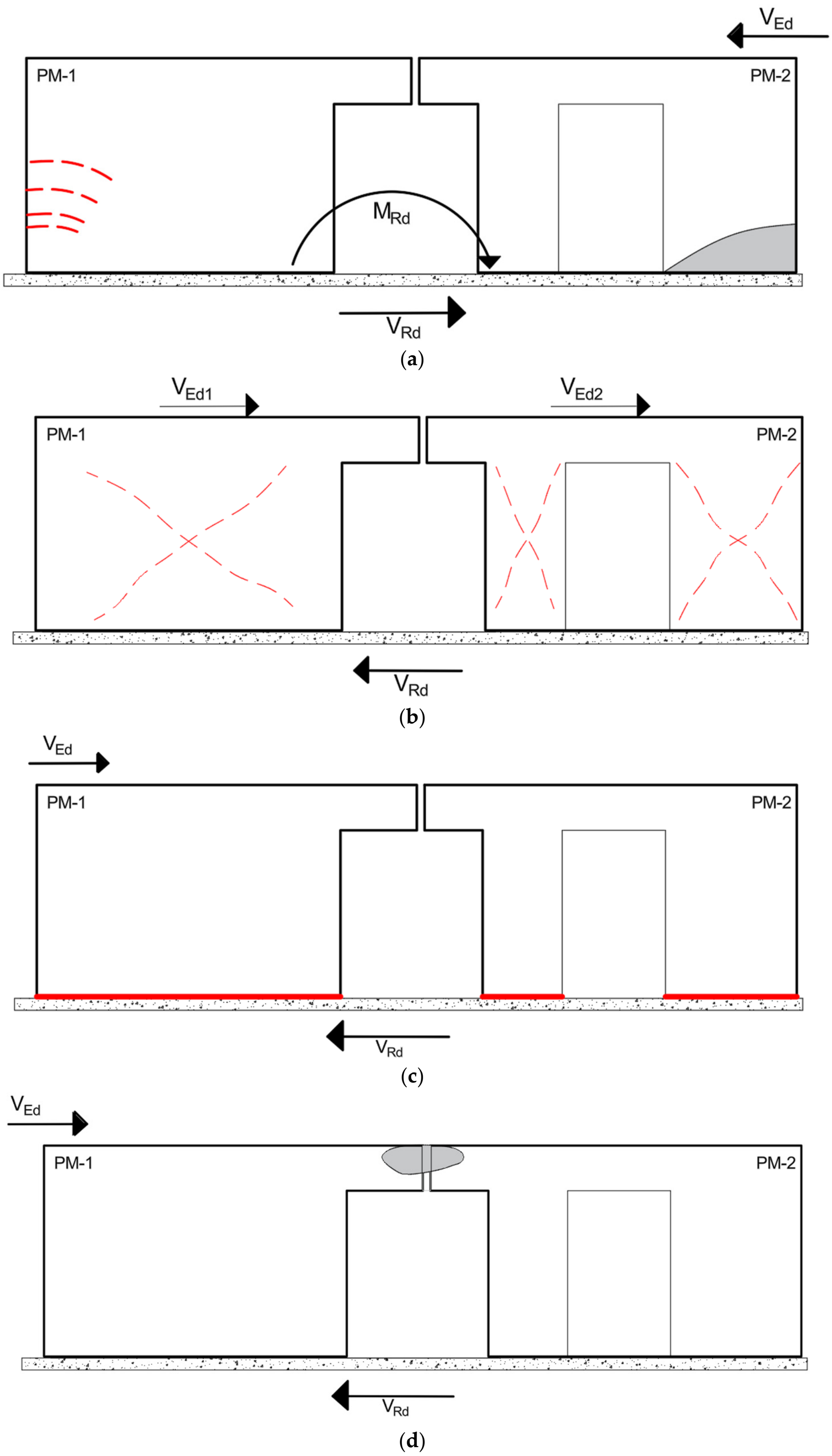

Figure 26. Failure mechanisms considered to determine the capacity of a wall assembly: (**a**) flexural failure at the base of a wall assembly; (**b**) simultaneous shear failure of wall panels PM-1 and PM-2; (**c**) shear failure of the wall assembly along horizontal joint J1 at the base; and (**d**) shear failure of the wall assembly at vertical joint D4.

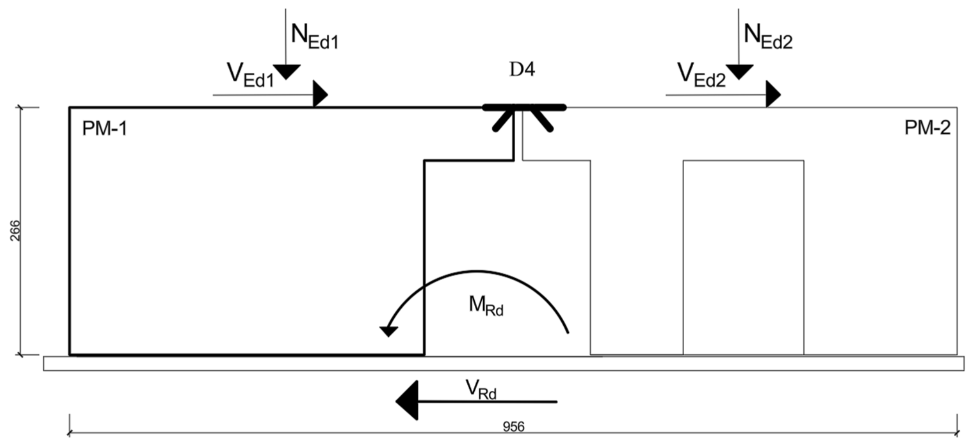

Figure 27. Wall assembly considered for moment resistance verification, showing panels PM-1 and PM-2 (all dimensions in cm).

The design shear forces at the base of the building (level 0) resulting from the global analysis were $V_{Ed1} = 432$ kN (panel PM-1) and $V_{Ed2} = 286$ kN (panel PM-2) (see Table 4). Assuming a similar axial force distribution in the two panels ($N_{Ed1} = N_{Ed2} = 427$ kN), the design forces in the wall assembly were determined as follows:

$$V_{Ed} = V_{Ed1} + V_{Ed2} = 718 \text{ kN}$$

$$N_{Ed} = N_{Ed1} + N_{Ed2} = 854 \text{ kN}$$

The corresponding design bending moment at the base was estimated as

$$M_{Ed} = M_{Ed1} + M_{Ed2} = 4646 + 3072 = 7718 \text{ kNm}.$$

The section considered for moment resistance verification includes both panels and the vertical end reinforcement (2Ø16), corresponding to reinforcement areas A_s and A'_s, as shown in Figure 28. Moment resistance of the wall assembly was evaluated using the procedure for walls with distributed and concentrated reinforcement described earlier in this section. The resulting moment resistance is equal to

$$M_{Rd} = 3879 \text{ kNm}.$$

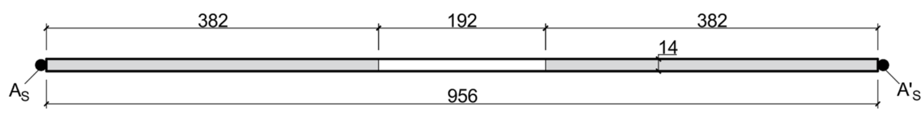

Figure 28. Cross-section of the wall-panel assembly used for moment resistance evaluation purposes, showing 2Ø16 vertical bars at each end (all dimensions in cm).

Note that M_{Rd} is significantly lower than the corresponding design bending-moment demand (M_{Ed}), indicating inadequate moment resistance. The resulting DCR value is

$$DCR = \frac{M_{Ed}}{M_{Rd}} = \frac{7718}{3879} = 1.99.$$

It is expected that the flexural failure mechanism of the wall-panel assembly is not critical for the seismic safety of the assembly in comparison with local mechanisms associated with the failure of panel connections, particularly those related to the vertical D4 joint, as discussed later in this section.

Shear force at the base of the assembly corresponding to the flexural failure mechanism can be determined by assuming that the resultant seismic force corresponding to M_{Rd} acts at the effective building height (equal to $2H/3$), with an overall building height of H = 15 m; hence,

$$V_{Rd1} = \frac{3M_{Rd}}{2 \cdot H} = 387.9 \text{ kN}.$$

6.2.2. Shear Resistance of the Wall Assembly Corresponding to a Simultaneous Shear Failure of Wall Panels PM-1 and PM-2

Shear resistance of an individual wall panel was discussed in Section 6.1, and a panel shear resistance of 101.6 kN was determined according to the relevant EC 2 provisions. A scenario corresponding to simultaneous shear failure of both panels is presented in Figure 26c, and the resulting shear resistance for the wall assembly is equal to

$$V_{Rd2} = 2 \cdot 101.6 = 203.2 \text{ kN}.$$

6.2.3. Sliding Shear Failure of the Wall Assembly Along a Horizontal Joint (J1) at the Base

Connection between the load-bearing wall panels, e.g., panels PM-1 and PM-2, and the foundation was established via a plain interface in the form of a 20 mm thick mortar layer (characteristic compression strength of 2.5 MPa) (see Figure 29). A similar mortar layer was also provided between the panel and the floor slab at upper floor levels. In accordance with EC 2 (Cl. 6.2.5), shear transfer across an interface such as joint J1 is achieved through a shear friction mechanism, which is based on Coulomb's Law. Since there is no continuous vertical reinforcement across the joint and the mortar layer has a very low strength, the cohesion component of the resistance was disregarded. Based on the original construction documentation, there is no evidence of interface roughening at the construction site. Therefore, the interface was conservatively classified as a "smooth surface" according to EN 1992-1-1 and the corresponding friction coefficient (μ = 0.6) was adopted.

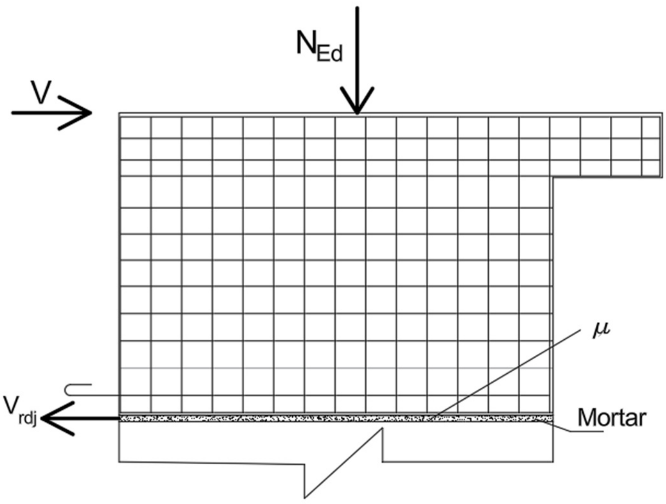

Figure 29. Joint J1 at the interface between wall panel PM-1 and the foundation achieved via a mortar layer.

The design shear resistance along joint J1 was determined as a product of the frictional coefficient (μ) and normal stress (σ_n) acting on the interface (area A_i) as follows:

$$V_{Rd} = \mu \cdot \sigma_n \cdot A_i \tag{32}$$

where the normal stress was determined based on the design axial force in the wall panel as follows:

$$\sigma_n = \frac{N_{Ed}}{A_i} = 0.8 \text{ MPa} < 0.6 f_{cd} \quad (33)$$

where the wall cross-sectional area at the joint location is $A_i = 53{\cdot}10^4$ mm^2 and the axial force is $N_{Ed} = 427$ kN. Since the resulting normal stress ($\sigma_n = 0.8$ MPa) from Equation (33) is less than the EC2-prescribed limit $0.6 f_{cd} = 6.4$ MPa, it can be expected that the crushing of the mortar layer is not going to control the behaviour.

The corresponding sliding shear resistance of wall panel PM-1 at joint J1 was determined according to Equation (32) as follows:

$$V_{Rd} = 256 \text{ kN}$$

It can be assumed that the sliding shear resistance for wall panel PM-2 is the same as for panel PM-1. Therefore, the sliding shear resistance of the wall assembly, as shown in Figure 26c, is equal to

$$V_{Rd3} = 2{\cdot}256 = 512 \text{ kN}.$$

6.2.4. Shear Resistance of the Wall Assembly Corresponding to the Failure of Joint D4

It is expected that the wall assembly may experience failure at joint D4, along either a horizontal or a vertical failure plane (see Figure 30a,b). Failure mechanisms along both planes are associated with a failure of the steel anchorage plate at joint D4. It should be noted that only panel PM-1 was considered in the determination of the DCR values related to the failure of joint D4. For that reason, panel PM-2 is shown with dashed lines in the diagram.

It is also important to note that for failure along the vertical plane (see Figure 30b), the horizontal shear force (V_{Rd}) shown in the diagram represents the strength-level force corresponding to the capacity along the vertical plane (N_{Rd}). In this case, the horizontal shear force is needed for the DCR calculations presented in Section 6.2.6.

The governing failure mechanism is characterized by the lowest resistance. Material properties of the connections were obtained from the original construction documentation, and the resistance (capacity) of the joint was evaluated in accordance with the applicable Eurocode requirements. Note that the assessment was performed only for joint D4; hence, the effect of failure at adjacent panel joints on the seismic response of the LPB structure was not considered. Examination of nonlinear behaviour of wall panels and their connections (including joint D4) is beyond the scope of this study.

The following possible failure mechanisms related to joint D4 are discussed further in Sections 6.2.5 and 6.2.6:

(a) Shear failure mechanisms along the horizontal plane (see Figure 30a):

SH1. Rupture of the welded steel-plate connection;
SH2. Tensile failure of the steel plate;
SH3. Tensile failure of the anchor bars; and
SH4. Weld failure at the anchor bar-to-plate connection.

(b) Shear failure mechanisms along the vertical plane (see Figure 30b):

SV1. Tensile failure of anchor bars and
SV2. Pullout failure of anchor bars.

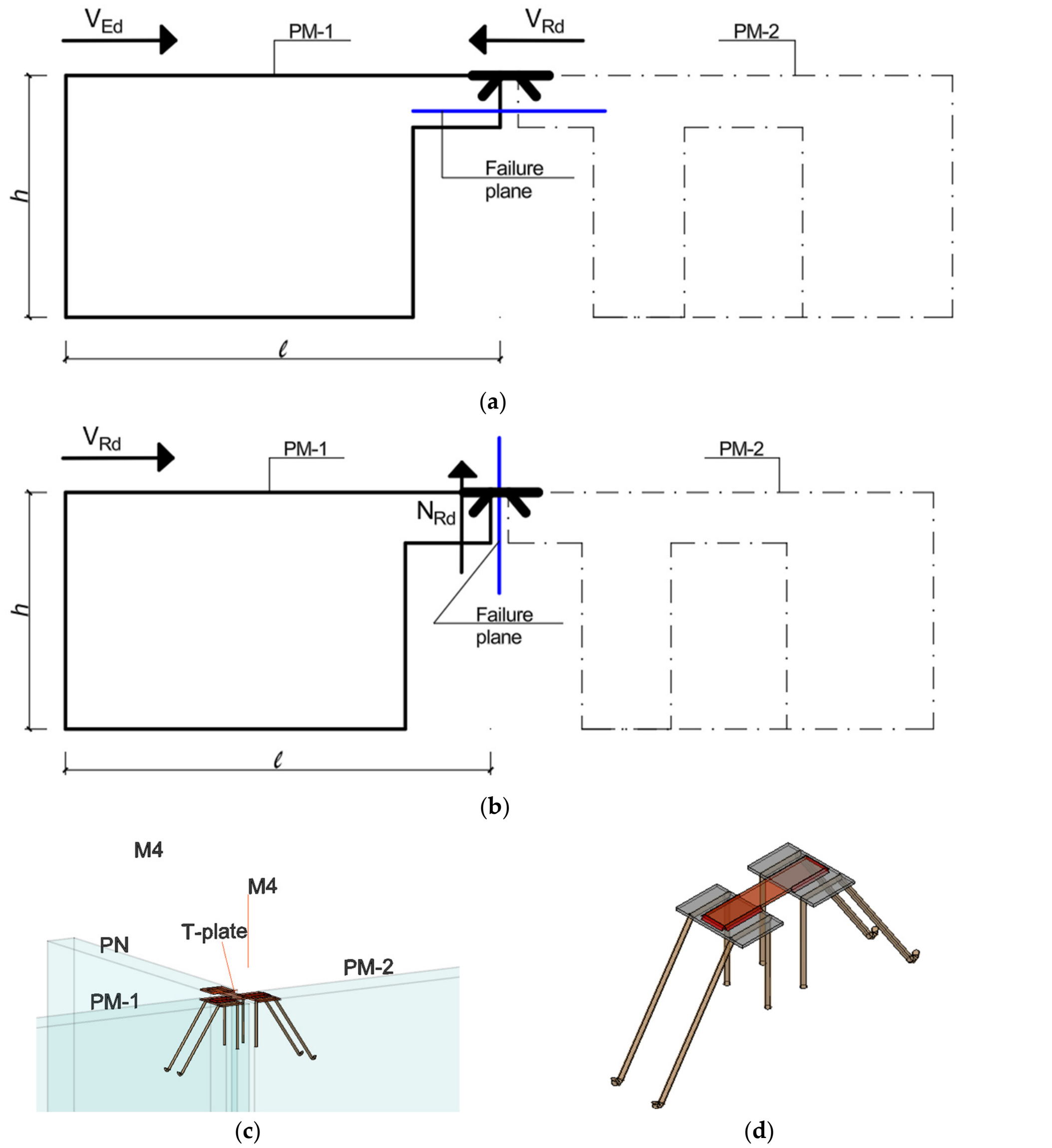

Figure 30. Joint D4: (**a**) horizontal failure plane; (**b**) vertical failure plane; (**c**) 3D view of joint D4 and the adjacent panels; (**d**) steel-plate connection for panels PM-1 and PM-2 (all dimensions in cm).

6.2.5. Shear Failure Mechanisms Along the Horizontal Plane of Joint D4

It should be noted that the shear capacity of joint D4 along the horizontal plane is based on only one active plate (M-4) and the related anchor bars. Four possible failure mechanisms (SH-1 to SH-4) are illustrated in Figure 26a and discussed in the following text.

(a) SH1 Rupture of the welded steel-plate connection

Figure 31 illustrates the T-shaped steel-plate connection between load-bearing wall panels PM-1 and PM-2 (shown in the vertical direction) and a non-loadbearing wall panel (PN, shown in the horizontal direction). It is assumed that seismic shear force (V) acts in the plane of panels PM-1 and PM-2. Plate A is the critical connecting plate and is subjected to tension due to force V, while plate B is welded to plate A in the perpendicular direction (along the length of panel PN). Since these two plates are connected along Section 1-1 (shown in Figure 31), it is expected that the welded connection between plates A and B may fail in shear before plates A and B experience shear failure.

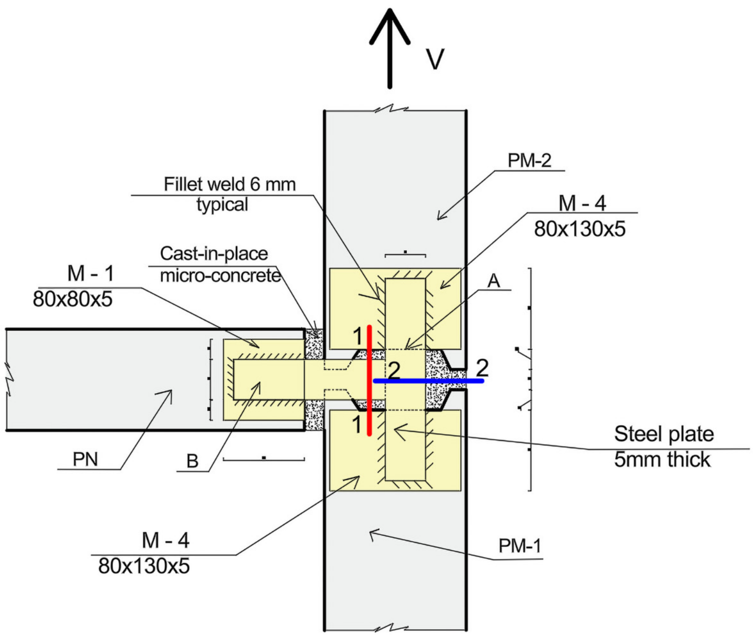

Figure 31. T-shaped steel-plate connection for panels PM-1, PM-2, and PN (all dimensions in mm).

Shear resistance of the weld was evaluated based on the effective weld area and the weld material's design shear strength and was determined according to EC 3 (Cl 4.5.2) [46] as follows:

$$V_{Rd,w} = A_w \cdot f_{vw,d} \tag{34}$$

An effective weld length of $l_w = 160$ mm was considered, corresponding to two 80 mm long weld segments parallel to the shear-transfer direction. For a fillet weld with a size of $h = 6$ mm and an effective throat thickness of $a = 0.7h$, the effective weld area is equal to

$$A_w = l_w \cdot a = 672 \text{ mm}^2.$$

The characteristic tensile strength of weld metal (electrode material) was taken as $f_u = 412$ MPa according to the KTP 10–78 code [47], while the modified mean tensile strength of weld metal used for the seismic assessment was $f_{um} = 305.2$ MPa (see Table 2, column 7). Finally, the design shear strength of weld metal was determined according to EC 3 (Cl. 4.5.3.3) as follows:

$$f_{vw,d} = \frac{f_{um}}{\sqrt{3}\beta_w \gamma_M} = 176.2 \text{ MPa},$$

where $\beta_w = 1.0$ and $\gamma_M = 1.0$ were used for assessment purposes. The resulting design shear resistance of the welded connection was determined according to Equation (34) as follows:

$$V_{Rd,w} = 118.4\text{kN}$$

(c) SH2 Tensile failure of the steel plate

It is expected that the tensile failure of the plate may take place along Section 2-2 (see Figure 31). Tensile resistance of a steel plate can be determined according to the following equation:

$$T_{Rd} = A_s \cdot f_{ym} \tag{35}$$

For the assessment of the existing structure, a modified mean steel yield strength of $f_{ym} = 155.5$ MPa was used (Table 2, column 7). Since the plate width is $w = 40$ mm and the thickness is $t = 5$ mm, it follows that

$$A_s = w \cdot t = 200\,\text{mm}^2,$$

and according to Equation (35),

$$T_{Rd} = 31.1\ \text{kN}.$$

Therefore, the shear resistance of the assembly corresponding to this failure mechanism is equal to

$$V_{Rd} = 31.1\ \text{kN}.$$

(c) SH3 Tensile failure of anchor bars

Figure 32 illustrates the configuration of steel plate M-4 and the arrangement of anchor bars that were welded to the plate and embedded into a wall panel. Under seismic loading, horizontal shear force applied to plate M-4 is resisted through tensile forces in the inclined and horizontal anchor bars.

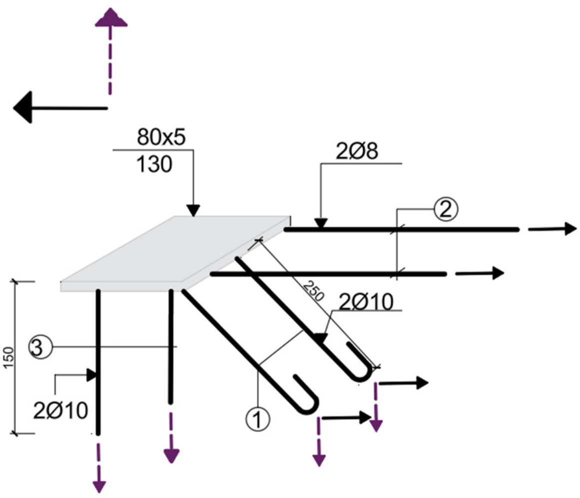

Figure 32. Steel-plate connection (M-4) subjected to horizontal and vertical shear forces resisted through tensile forces in the anchor bars (horizontal and vertical components of forces shown in the diagram; however, welds are not shown) (all dimensions in mm).

The tensile resistance of the anchor bars was determined according to the EC 2 requirements as a product the reinforcement area and the modified mean steel yield strength as follows:

$$N_{Rd} = A_s \cdot f_{ym} \tag{36}$$

Only reinforcement bars "1" and "2" were taken into account in this assessment because they are able to provide tensile resistance in the horizontal plane (the forces are shown by solid lines in Figure 32). A modified mean steel strength of $f_{ym} = 251.9$ MPa (Table 2, column 7) was used for assessment purposes, and the corresponding reinforcement areas are equal to

$$A_{s1} = 157\ \text{mm}^2\ (2\varnothing10)$$

$$A_{s2} = 100\ \text{mm}^2 (2\varnothing8).$$

The resulting tensile resistance due to bars "1", inclined at a 45° angle with respect to the horizontal axis, and horizontal bars "2", was estimated according to Equation (36) as follows:

$$N_{Rd} = (A_{s1} \cdot cos45^\circ + A_{s2}) f_{ym} = 53.1\ \text{kN}.$$

Therefore, the shear resistance of the assembly corresponding to this failure mechanism is equal to

$$V_{Rd} = 53.1\ \text{kN}.$$

(d) SH4 Weld failure at the anchor bar-to-plate connection

Weld failure at the anchor bar-to-plate connection was evaluated considering only the welded connection for anchor bars "1" (2∅10) (note that the welded connection is omitted from Figure 32). The evaluation procedure is the same as for mechanism SH1. Each bar was attached to the steel plate by means of two fillet welds, with an effective weld length of $l_w = 80$ mm on each side of the bar, a 5 mm size (h), and an effective throat thickness of $a = 0.7h$. The modified mean tensile strength of the weld metal was 305.2 MPa (see Table 2, column 7), and the design shear strength of the weld metal ($f_{vw,d}$) was 176.2 MPa. The effective weld area for each bar, corresponding to two welds, is equal to

$$A_w = 2(l_w \cdot a) = 560 \text{ mm}^2.$$

The design shear resistance for two welded bars was determined according to Equation (34) as follows:

$$V_{Rd} = 2\left(560 \text{ mm}^2\right)(176.2\text{MPa}) = 197.4\text{kN}$$

(e) Governing failure mechanism

The following shear resistance values were obtained for the mechanisms considered in this section:

SH1. Rupture of the welded steel plate connection: $V_{Rd} = 118.4$ kN;
SH2. Tensile failure of the steel plate: $V_{Rd} = 31.1$ kN;
SH3. Tensile failure of the anchor bars: $V_{Rd} = 53.1$ kN;
SH4. Weld failure at the anchor bar-to-plate connection: $V_{Rd} = 197.4$ kN.

A comparison of these values indicates that the lowest resistance is associated with the tensile failure of the steel plate (mechanism SH2); hence, the governing shear capacity of the joint D4 in the horizontal plane is equal to

$$V_{Rd} = \min(118.4, 31.1, 53.1, 197.4) = 31.1 \text{ kN}.$$

6.2.6. Shear Failure Mechanisms Along the Vertical Plane of Joint D4

It should be noted that the shear capacity of joint D4 in the vertical plane was determined based on a single steel plate (M-4). Failure of joint D4 along the vertical plane is illustrated in Figure 30b, and two possible failure mechanisms (SV1 and SV2) are discussed in the following text.

(a) SV1 Tensile failure of anchor bars

Tensile resistance of the anchor bars in the vertical plane was evaluated by considering only bars "1" (2∅10) and "3" (2∅10), as illustrated in Figure 32. The tensile resistance was determined in accordance with the EC 2 provisions. For inclined anchor bars "1", the resistance was equal to the sum of vertical components of tensile forces developed in each bar. The tensile resistance in the vertical direction was determined according to Equation (36) as follows:

Bars "1": area $A_{s1} = 157$ mm^2

$$N_{Rd1} = A_{s1} \cdot f_{ym} \cdot \sin 45^\circ = 27.92 \text{ kN}$$

Bars "3": area $A_{s3} = 157$ mm^2

$$N_{Rd3} = A_{s3} \cdot f_{ym} = 39.58 \text{ kN}$$

A modified mean steel strength of $f_{ym} = 251.9$ MPa (Table 2, Column 7) was used, and the total tensile resistance was determined as follows:

$$N_{Rd} = N_{Rd1} + N_{Rd3} = 67.5\text{kN}$$

(b) SV2 Pullout failure of anchor bars

Pullout failure of the anchor bars connected to plate M-4 may take place due to insufficient anchorage length and a loss of bond between the bars and the concrete. The plate-and-anchor layout is presented in Figure 32. Inclined anchor bars "1" (2Ø10) with a 250 mm anchorage length and anchor bars "2" (2Ø10) with a 150 mm anchorage length were considered for this assessment. Bars "1" have 180° hooks at the ends; however, the effect of the hooked anchorage was neglected in the calculations.

The full tensile resistance of the anchor bars ($T_{Rd,\ max}$) was first determined assuming the full tensile resistance, which corresponds to an anchorage length (l_b) greater than the required anchorage length (l_{brqd}). For assessment purposes, a modified mean steel yield strength of $f_{ym} = 251.9$ MPa (Table 2, Column 7) was used, and the bar area (10 mm diameter) was $A_s = 78.5$ mm^2. Therefore, $T_{Rd,\ max}$ was determined according to the following equation (for two Ø10 anchor bars):

$$T_{Rd,max} = 2 \cdot A_s \cdot f_{ym} = 39.55 \text{ kN}$$

The required anchorage length for a reinforcement bar with a diameter of $\varnothing$ was determined according to EC 2 (Cl. 8.4.3) as follows:

$$l_{b,rqd} = \frac{\varnothing}{4} \frac{\sigma_{sd}}{f_{bd}} \tag{37}$$

where σ_{sd} is the design stress of the reinforcing bar at the position from which the anchorage is measured. Assuming that the bar develops its design yield strength, $\sigma_{sd} = f_{ym} = 251.9$ MPa. The design bond stress (f_{bd}) was determined according to EC 2 (Cl. 8.4.2) as follows:

$$f_{bd} = 2.25\, \eta_1\, \eta_2\, f_{ctd}, \tag{38}$$

where $\eta_1 = 0.7$ is a coefficient related to bond conditions (assuming a poor bond condition) and $\eta_2 = 1$ is a coefficient related to bar diameter ($\varnothing \leq 32$mm). Note that for C16/20 concrete f_{ctd} = design tensile strength of concrete (EC 2 Cl. 3.1.6), however the modified mean tensile strength was used for the calculations (see Table 2, column 7), hence $f_{ctd} = 1.41$ MPa. Finally, the design bond stress from Equation (38) is equal to

$$f_{bd} = 2.22 \text{ MPa}.$$

and the required anchorage length from Equation (37) is equal to

$$l_{b,rqd} = \frac{}{4} \frac{\sigma_{sd}}{f_{bd}} = 284 \text{ mm}.$$

Both bars "1" and "3" have an anchorage length of less than 284 mm; therefore, it can be expected that these bars cannot attain the full tensile resistance. The maximum tensile force that can be developed in two bars with diameter of Ø and anchorage length of l_b is equal to

$$F_{bd} = 2 \cdot f_{bd} \cdot (\pi \cdot \phi \cdot l_b). \tag{39}$$

For bars "3", with an anchorage length of $l_b = 150$ mm, the maximum tensile force based on Equation (39) is

$$F_{bd3} = 20.92 \text{ kN}.$$

Similarly, the maximum tensile force for bars "1" with an anchorage length of $l_b = 250$ mm according to Equation (39) is equal to

$$F_{bd1} = 34.88 \text{ kN}.$$

Consequently, the maximum tensile resistance (pullout resistance) for the anchor bars in the vertical plane is equal to the anchorage force; hence,

$$N_{Rd} = F_{bd1} \cdot sin\, 45^{\circ} + F_{bd3} = 45.6 \text{ kN}$$

(c) Governing failure mechanism

The shear resistance of joint D4 in the vertical plane was determined by considering the following failure mechanisms:

SV1. Tensile failure of anchor bars: $N_{Rd} = 67.5$ kN;
SV2. Pullout failure of anchor bars: $N_{Rd} = 45.6$ kN.

The governing shear resistance of joint D4 in the vertical plane was therefore determined as

$$N_{Rd} = \min(67.5, 45.6) = 45.6 \text{ kN}.$$

It can be concluded that the shear resistance of joint D4 in the vertical plane is governed by the pullout failure of anchor bars.

Let us consider the equilibrium of forces in panel PM-1 (see Figure 30b). The bending moment corresponding to the shear resistance (N_{Rd}) along the vertical plane is equal to the bending moment created by the corresponding horizontal shear force (V_{Rd}) as follows:

$$V_{Rd} \cdot h = N_{Rd} \cdot l \tag{40}$$

where $l = 4.78$ m is the length at the top of panel PM-1 and h = 2.66 m is the height of the panel. Equation (40) can be used to determine the horizontal shear force (V_{Rd}) as follows:

$$V_{Rd} = \frac{N_{Rd} \cdot l}{h}$$

Since $N_{Rd} = 45.6$ kN, the horizontal shear force associated with failure along the vertical plane is equal to

$$V_{Rd} = 81.9 \text{ kN}.$$

6.2.7. Governing Shear Resistance for Joint D4

The shear resistance of joint D4 was evaluated by considering its resistance along both vertical and horizontal failure planes. The shear resistance along the horizontal plane is $V_{Rd} = 31.1$ kN, while the shear resistance corresponding to failure along the vertical plane is $V_{Rd} = 81.9$ kN. Since the resistance corresponding to the horizontal plane is lower, it can be concluded that the governing shear resistance for joint D4 is

$$V_{Rd} = 31.1 \text{ kN}.$$

A conceptual summary of the potential failure mechanisms for joint D4 along both the horizontal and vertical planes is presented in Figure 33, and the corresponding DCR values are summarized in Table 6.

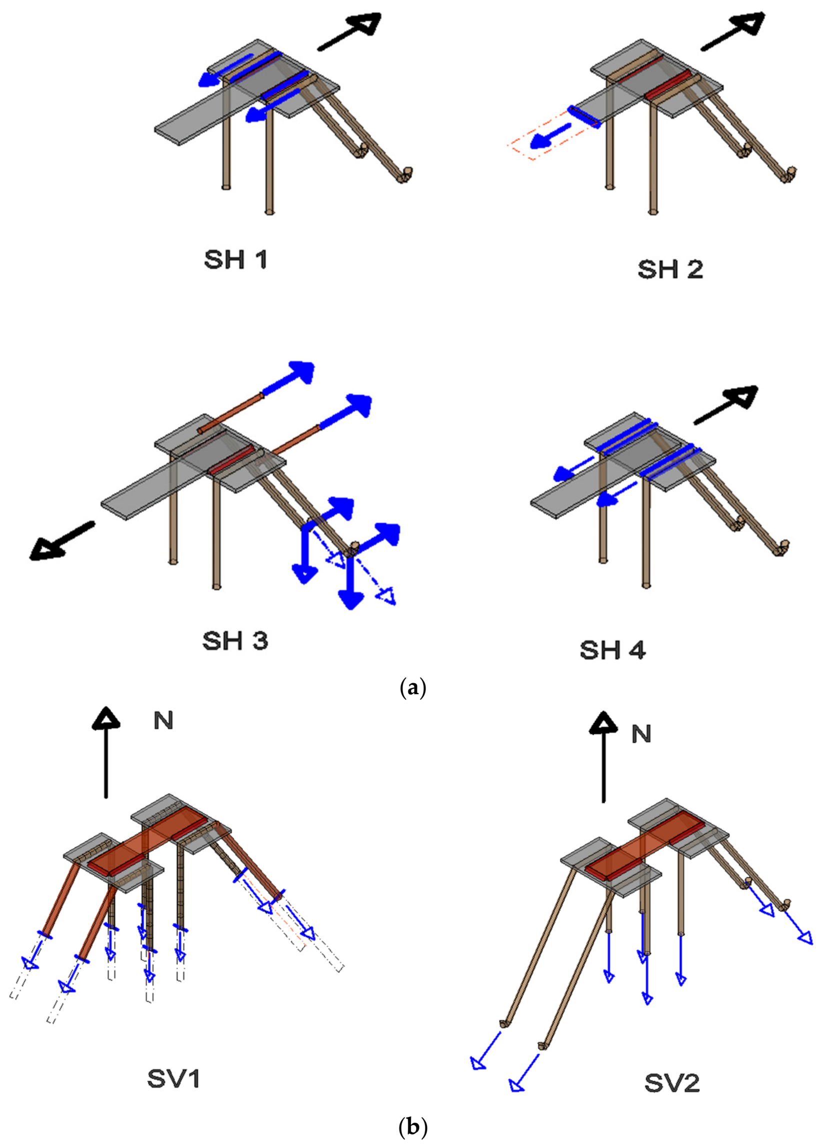

Figure 33. Conceptual failure mechanisms for joint D4: (**a**) horizontal plane; (**b**) vertical plane.

Table 6. Failure mechanisms for joint D4: a summary of the seismic assessment results ($a_{gr} = 0.293$ g and $q = 1.5$).

No.	Failure Mechanism	Shear Resistance (Capacity, C) (kN)	Seismic Shear Demand (D, kN)	Demand/ Capacity Ratio (DCR)
1	SH1	118.4	432	3.65
2	SH2	31.1	432	13.89
3	SH3	53.1	432	8.14
4	SH4	197.4	432	2.19
5	SV1	121.3	432	3.56
6	SV2	81.9	432	5.27

6.2.8. Summary of Seismic Assessment Results for the Wall Assembly

Four possible failure mechanisms for the wall assembly considered in this study are presented in Figure 26 and the corresponding shear capacities, demands, and DCR values are summarized in Table 7. Note that for mechanisms 1, 2, and 3, the DCRs were determined based on the joint shear demand for panels PM-1 and PM-2 because these mechanisms assumed that these panels are joined through joint D4 and act together as a single structure.

Table 7. Failure mechanisms for the wall-panel assembly: a summary of the seismic assessment results.

No.	Failure Mechanism	Shear Resistance (Capacity, C) (kN)	Seismic Shear Demand (D, kN)	Demand/ Capacity Ratio (DCR)
1	Flexural failure at the base	$V_{Rd1} = 387.9$ kN	718	1.85
2	Simultaneous shear failure of the wall panels	$V_{Rd2} = 203.2$ kN	718	3.53
3	Sliding shear failure along horizontal joint J1	$V_{Rd3} = 512.0$ kN	718	1.4
4	Shear failure of vertical joint D4 (horizontal plane)	$V_{Rd4} = 31.1$ kN	432	13.89

On the other hand, mechanism 4 considers the failure mechanism for joint D4, and for that reason, the DCR was determined based on capacity and demand for panel PM-1 only; this was also explained in Section 6.2.4.

A comparison of the calculated DCRs for the failure mechanisms of the wall-panel assembly indicates that vertical joint D4 is critical for shear failure of the wall assembly. This finding highlights the importance of connection details in the seismic performance of the case-study LPB. However, it should be noted that the linear elastic seismic analysis procedures used in the study enables only a comparison of the investigated failure mechanisms based on the elastic seismic demand and do not explicitly simulate the actual sequence of failure mechanisms.

7. Discussion

This section outlines limitations of the current study and needs for future studies; qualitative validation of the findings based on the damage observations after the 2019 Durres, Albania, earthquake; and a sensitivity analysis for obtained seismic assessment results related to selected failure mechanisms.

7.1. Limitations of the Current Study

This study has several limitations that need to be considered in future studies, as discussed below:

(a) The study is focused on a specific LPB typology, which is widespread in urban areas of Albania; however, it should be recognized that other LPB typologies (or other variants of the same typology) may exist. Therefore, the findings of this study are primarily related to the building typology and construction details presented in this manuscript. Further research studies are needed to establish whether the findings of this study may be applicable to other LPB typologies in Albania and Eastern European countries.

(b) Seismic assessment performed in this study was based on the results of linear elastic seismic analyses, including ESA and RSA, which are not able to simulate the nonlinear structural responses of buildings exposed to damaging earthquakes. However, since the information related to the condition and materials used for construction of the case-study building was not available, according to the EC 8-3 provisions, seismic assessment may be performed using linear elastic seismic analysis procedures only (there is no need to perform nonlinear analyses).

(c) The adopted linear elastic seismic assessment procedures were not able to capture stiffness degradation, damage progression, force redistribution, and/or post-yield behaviour following the failure of individual connections or wall panels. Code-based DCR checks were performed for selected structural elements (wall panels and wall assemblies), and the reported DCR values should be interpreted as a comparative assessment of the investigated failure mechanisms rather than a prediction of the actual failure sequence. In addition, the influence of uncertainties related to the assumed connection stiffness value on the global seismic response and local force distribution was not investigated in the present study. Nonlinear seismic analyses at the component or assembly level are recommended to gain insight into progressive failure mechanisms for the building and the effect of nonlinear connection behaviour on the global response.

(d) The effect of underlying soil properties was simulated through linear elastic soil springs, while more advanced nonlinear SSI aspects were not considered. It is recommended that nonlinear SSI effects, including foundation uplift and potential loss of contact between the foundation and the supporting soil under seismic loading, be considered in future studies.

(e) Stiffness properties of exterior façade panels were not considered in the 3D numerical model; however, their masses were considered in the seismic weight calculations. Although these panels are non-load-bearing elements, their contribution to the overall lateral stiffness may influence the global seismic response. The interaction of wall panels and their out-of-plane behaviour were beyond the scope of the present study.

(f) Torsional effects were not considered in the ESA, and accidental torsion was not accounted for in the 3D numerical model used for the RSA.

(g) The RSA was performed using the SRSS modal combination; however, since the first two vibration periods are relatively close, the application of the Complete Quadratic Combination (CQC) method would result in a more accurate representation of modal response, so it should be used in future studies on LPBs with similar dynamic characteristics.

(h) Another limitation of the present study is that the stiffness properties assigned to the FE59 and KE55 joint elements in the LIRA-SAPR module were adopted based on the available design information and were idealised using equivalent elastic spring properties. The influence of uncertainties in these stiffness values on the global dynamic characteristics of the numerical model (e.g., vibration periods), torsional response, and seismic force distribution was not investigated. A dedicated stiffness sensitivity study considering plausible variations in joint stiffness values would provide additional insight into the accuracy of the predicted forces and is recommended for future research studies.

7.2. Qualitative Validation of the Findings Based on the Observed Earthquake Damage

In spite of the above stated limitations, the findings of this study proved to be in agreement with observations following recent earthquakes in Albania, such as the 26 November 2019 Durrës earthquake (Mw 6.4). A building of the same typology as the investigated building, located in the Kombinat area of Tirana (see floor plan in Figure 34a), exhibited significant localized damage at vertical joint D4 (see Figure 34b,c). The seismic assessment performed in this study identified the shear capacity of the same joint as critical for the seismic safety of the investigated wall assembly, with the largest DCR of 13.89. It should be noted that no damage was observed in the panel. Although earthquake damage observations cannot be fully interpreted without a detailed post-earthquake assessment of the investigated building, the correspondence between the observed damage pattern and the location shows very good qualitative agreement with the findings of the current study.

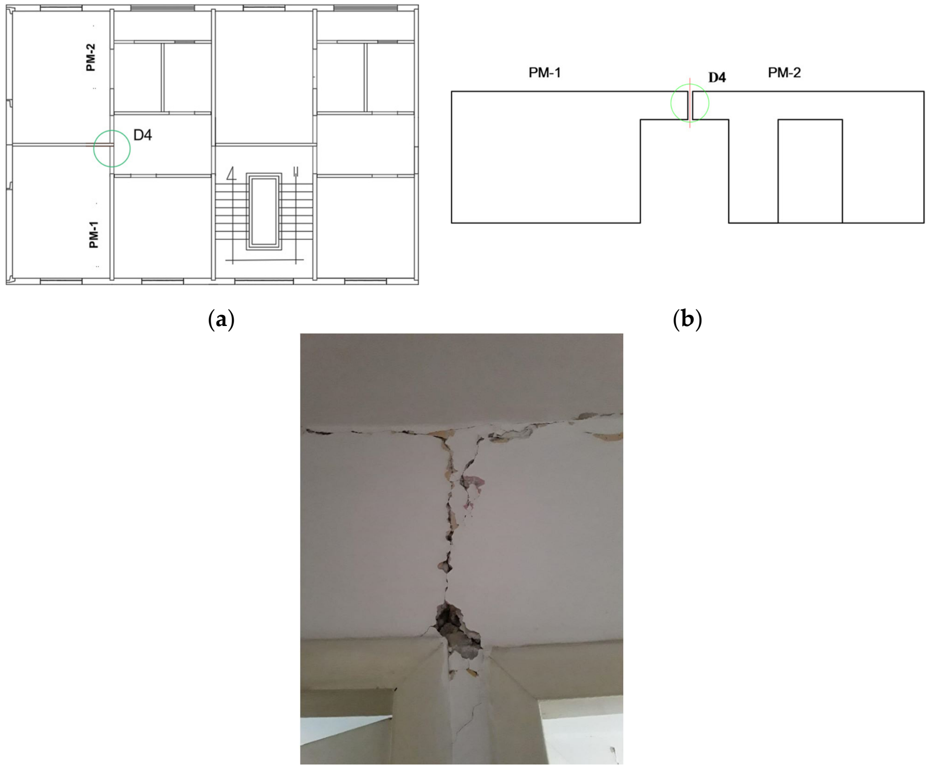

(**a**) (**b**)

(**c**)

Figure 34. A damaged LPB building in Tirana due to the 26 November 2019 earthquake (Mw 6.4): (**a**) floor plan showing the location of damaged vertical joint D4; (**b**) vertical elevation of the wall assembly, showing the joint location; (**c**) observed earthquake damage.

There is uncertainty related to some of the input parameters used for the seismic assessment of the case-study building, mostly those that depend at the assembly stage, e.g., the composition and strength of the mortar at the wall-to-foundation interface (horizontal joint J1) and the quality/strength of the welds at vertical joint D4. It is expected that the mechanical properties of concrete and steel used for construction of precast RC panels at the off-site manufacturing plant were more controlled; however, the material properties specified in the original construction documentation are uncertain (in situ material testing information would be very useful).

7.3. Sensitivity Analysis

A sensitivity analysis was performed to get insight into the possible range of assessment results depending on the input parameters. Since in situ material testing was not performed for the case-study building, it was deemed appropriate to perform a sensitivity analysis related to the seismic assessment of joint D4. The characteristic material properties used for the seismic assessment were reduced by applying an appropriate confidence-factor (*CF*) value (1.35) to reflect the knowledge level (KL1) per EC 8-3 provisions, as discussed earlier in the manuscript. A behaviour factor (q) of 1.5 was used for the seismic assessment, in accordance with the EC 8-3 requirements, while a higher behaviour-factor (q) value of 3.0 was also considered in the sensitivity study (as a reference related to the design of new buildings). Finally, a lower seismic hazard level (a_{gR} = 0.12 g) was considered to reflect previous seismic hazard requirements for Albania, while the current seismic hazard value

(a_{gR} = 0.293 g) was used for seismic assessment purposes. A summary of the parameters considered in the sensitivity analysis is presented in Table 8.

Table 8. Summary of input parameters for seismic sensitivity analysis of joint D4.

No.	Material Strength	Behaviour Factor (q)	Design Acceleration a_{gR} (g)
1	Characteristic	3.0	0.293
2	Characteristic	1.5	0.293
3	Characteristic	3.0	0.12
4	Modified/reduced	3.0	0.293
5 *	Modified/reduced	1.5	0.293
6	Modified/reduced	1.5	0.12

Notes: *—reference case for seismic assessment in this study, based on the EC 8-3 requirements.

The results of the sensitivity analysis are presented in Figure 35 in the form of DCR values for the four failure mechanisms along the horizontal plane (SH1 to SH4); refer to Section 6.2.5 for detailed calculations. It can be seen from the chart that the variation in input parameters did not affect the conclusions. For the case where the behaviour factor (q) is 1.5 (No. 5), the governing failure mechanism is SH2, corresponding to a DCR of 13.89. Note that the conclusion would be the same for other cases related to failure mechanism SH2 based on the high DCR values.

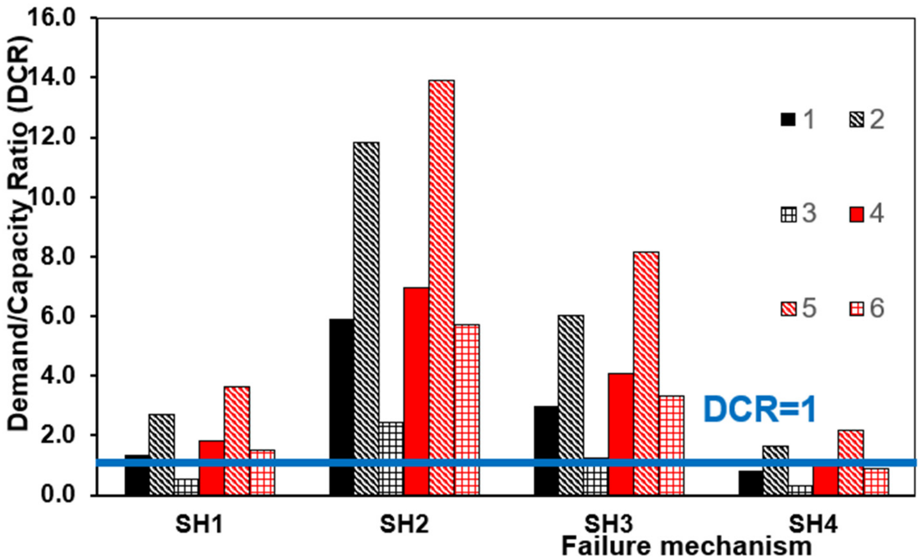

Figure 35. Sensitivity analysis for seismic assessment of joint D4 (failure mechanisms SH1 to SH4 along the horizontal plane).

Although a sensitivity analysis was not performed for all failure mechanisms related to the wall assembly under consideration, it is expected that the results would show a similar trend. For example, seismic assessment performed in the current study showed a DCR value of 1.4 for sliding shear failure along joint J1 (shown as No. 3 in Table 7). Since the shear capacity for sliding shear failure depends on the value of the frictional coefficient, it would be possible to obtain a higher (less favourable) DCR value, should the frictional coefficient be lower than the adopted value of 0.6.

8. Conclusions

This manuscript presents a seismic assessment of an existing five-storey LPB in Tirana, Albania. LPBs were used for the construction of multi-family residential buildings in the 1970s and 1980s, and they account for a significant fraction of the existing urban building stock in Albania. Seismic analyses in this study were performed according to the requirements of the current Albanian seismic design code (KTP-N.2-89) and the Eurocode 8 framework (including EC 8-1 and EC 8-3). Two different seismic hazard levels were considered: the lower value (0.12 *g*) reflects the requirements of the previous seismic hazard map, while the higher value (0.293 g) reflects the updated seismic hazard requirements, which are currently used for design of new buildings in Tirana. The seismic response of the building was assessed in terms of the force and displacement demands. Subsequently, seismic assessment of a sample wall panel and a wall assembly was performed in terms of the Demand-to-Capacity ratio (DCR) to identify the extent of seismic deficiencies in precast RC structural elements and their connections. The following conclusions were derived based on the results of this study:

1. The assessment of structural capacity based on linear elastic seismic analyses (ESAs) indicated that the wall-panel connections are the most critical components of the investigated wall-panel assembly. When the assessment was performed according to the EC 8-3 requirements, with the updated seismic hazard level and a reduced behaviour factor (q) of 1.5, the representative wall panel (PM-1) was found to be deficient in both flexure and shear, with a flexural DCR of 5.13 and a shear DCR of 4.25. At the wall-assembly level, the governing failure mechanism was associated with brittle shear failure of vertical panel joint D4, with a DCR of 13.89 (Table 7). It is expected that the original seismic design of these buildings was performed without considering a desirable, flexure-governed ductile failure mechanism for structural elements and their connections. As a result, the shear capacity of the wall-panel connections proved to be inadequate for the given seismic design parameters, and brittle shear failure of the wall assembly due to seismic actions may be expected.
2. The integrity of the welded connections of precast RC wall panels proved to be a critical factor governing the seismic performance of the investigated wall assembly in the case-study LPB. The results show that the wall assembly under consideration could experience a shear failure of vertical joint D4, corresponding to a DCR of 13.89 for the EC 8-3 requirements with a behaviour factor (q) of 1.5. Therefore, it is important to survey the damage state of wall-panel joints in post-earthquake assessments of LPBs in order to identify buildings that may require seismic rehabilitation or retrofitting.
3. The updated Albanian seismic hazard map shows a significant increase in the seismic demand for the case-study building. When a lower design ground acceleration (0.12 g) was used, a seismic base shear of 1257 kN was obtained according to the EC 8-1, with a behaviour factor (q) of 3.0; however, when the updated Albanian seismic hazard map was used (with design acceleration of 0.293 g), the base shear increased by approximately 144% to 3070 kN; this is similar to the ratio of corresponding accelerations, that is, 0.293 g/0.12 g = 2.44. It was also found that the ESA, performed according to both the KTP-N.2-89 and EC 8-1 codes, produced comparable seismic forces (1276 kN and 1257 kN, respectively) for the same design PGA of 0.12 g and q of 3.0. The seismic base shear force determined according to the EC 8-3 requirements, using a behaviour factor (q) of 1.5, was 6140 kN, which is twice the value (3070 kN) obtained from the analysis performed using a q value of 3.0. This finding indicates that the ESA, performed according to the Albanian code and Eurocode 8, results in very similar global seismic demand for the same seismic design parameters. Due to a substantial increase in the seismic hazard level reflected in the 2019 seismic hazard maps, combined with a lower q value of 1.5 for existing RC buildings prescribed by EC 8-3, it is expected that many existing LPBs may not comply with the EC 8-3 requirements and may need to be retrofitted. Broader conclusions regarding the existing LPBs in

Albania require seismic research studies of larger building portfolios, including field surveys, material testing, and probabilistic analyses.

4. A comparison of the seismic analysis results for an ESA performed using a simple shear beam dynamic model of a five-storey LPB building and an RSA performed using a 3D FE model of the same building was useful for understanding the differences in the dynamic characteristics and seismic response results. For example, a shear beam model of the case-study building used for the ESA was assigned a fundamental period of 0.38 s obtained from the EC 8-1 empirical estimate, whereas a higher period (0.60 s) was obtained from the modal analysis of a 3D model in the LIRA-SAPR module. The results show that the 3D numerical model is more flexible; this could be attributed to the flexibility of connections, which was accounted for in the 3D model but was not considered in the shear beam model. It is also important to observe that the seismic base shear force obtained from the ESA using the shear beam model (3070 kN) was 13% lower than the corresponding value of 3524 kN obtained from the RSA performed using 3D FE model. The results indicate that preliminary seismic assessment of regular mid-rise LPBs such as the case-study building could be performed using ESA with a reasonable level of accuracy.

This study is expected to contribute to the improved understanding of the seismic response of LPBs and inform planning of future seismic rehabilitation or retrofitting projects. The findings may be applicable to other existing LPBs in Albania and Eastern European countries with similar construction details and structural features, provided that building-specific information, field survey data, and in situ material testing data are available.

Author Contributions: F.K.: Formal analysis, Investigation, Data curation, Writing–original draft, and Writing–review and editing; M.G.: Investigation, Validation, Supervision, and Writing–review and editing; S.B.: Conceptualization, Methodology, Validation, Supervision, and Writing–review and editing. All authors have read and agreed to the published version of the manuscript.

Funding: This research received no external funding.

Data Availability Statement: The original data presented in the study are openly available at https://doi.org/10.5281/zenodo.19564123. The repository contains the calculation spreadsheets supporting the seismic base shear calculations according to EC 8 and KTP-N.2-89, load combination, and LIRA-SAPR input parameters.

Acknowledgments: The authors acknowledge the Central Technical Construction Archive (AQTN), Tirana, for providing information on large-panel buildings in Albania. The first author acknowledges Ornela Şen, Polis University, Tirana, for her support. The authors also acknowledge valuable feedback provided by Ivan Milicević, Faculty of Civil Engineering, University of Belgrade. The authors gratefully acknowledge the technical support provided by the LIRA-SAPR team.

Conflicts of Interest: The authors declare no conflicts of interest.

References

1. United Nations Industrial Development Organization (UNIDO). Building Construction under Seismic Conditions in the Balkan Region. In *Design and Construction of Prefabricated Reinforced Concrete Building Systems*; United Nations Industrial Development Organization: Vienna, Austria, 1985; Volume 2.
2. Novikova, A.; Szalay, Z.; Simaku, G.; Thimjo, T.; Salamon, B.; Plaku, T.; Csoknyai, T. The Typology of the Residential Building Stock in Albania and the Modelling of Its Low-Carbon Transformation. In *Project SLED*; Regional Environmental Center for Central and Eastern Europe: Vienna, Austria, 2015.
3. Krosi, F. A Comprehensive Methodology for the Refurbishment of Large Panel Buildings. Focus on the Energy Efficiency and Non-Structural Intervention on the Building Envelope. Ph.D. Thesis, Polis University, Tirana, Albania, University of Ferrara, Ferrara, Italy, 2025.

4. Geological Survey of Albania. Geological & Seismic Hazard. Available online: https://www.geo.edu.al/Natural_Hazards/Geological_Seismic_Hazard/ (accessed on 13 May 2026).
5. *EN 1998-1*; Eurocode 8—Design of Structures for Earthquake Resistance-Part 1: General Rules, Seismic Actions and Rules for Buildings. European Committee for Standardization (CEN): Brussels, Belgium, 2005.
6. World Bank. *M6.4 Albania Earthquake Global Rapid Post Disaster Damage Estimation (GRADE) Report*; GPURL D-RAS Team; World Bank: Washington, DC, USA, 2019.
7. Guri, M.; Brzev, S.; Lluka, D. Performance of Prefabricated Large Panel Reinforced Concrete Buildings in the November 2019 Albania Earthquake. *J. Earthq. Eng.* **2022**, *26*, 5799–5825. [CrossRef]
8. Akademia e Shkencave e RPS të Shqipërisë. *Kusht Teknik Projektimi për Ndërtimet Antisizmike*; KTP-N.2-89; Ministria e Ndërtimit: Tirana, Albania, 1989.
9. *EN 1998-3*; Eurocode 8—Design of Structures for Earthquake Resistance-Part 3: Assessment and Retrofitting of Buildings. European Committee for Standardization (CEN): Brussels, Belgium, 2005.
10. Fattal, G.; Simiu, E.; Culver, C. *Observations on the Behavior of Buildings in the Romania Earthquake of March 4, 1977*; NBS Special Publication 490; U.S. Department of Commerce, National Bureau of Standards: Washington, DC, USA, 1977.
11. Bostenaru, M.D.; Sandu, I. *Precast Concrete Panel Apartment Buildings; Housing Report # 83; World Housing Encyclopedia*; Earthquake Engineering Research Institute (EERI) & International Association for Earthquake Engineering (IAEE): Oakland, CA, USA, 2002.
12. Khakimov, S.; Nurtaev, B. *Precast Reinforced Concrete Frame Panel System of Seria IIS-04. Report #66, World-Housing Encyclopedia*; Earthquake Engineering Research Institute: Oakland, CA, USA, 2002; Available online: https://www.world-housing.net (accessed on 18 August 2026).
13. Wyllie, L.A.; Lew, H.S. Performance of Engineered Structures, Chapter 6. In *Armenia Earthquake Reconnaissance Report (Special Supplement to Earthquake Spectra)*; Wyllie, L.A., Jr., Filson, J.R., Eds.; Earthquake Engineering Research Institute: Oakland, CA, USA, 1989; Volume 5, pp. 70–92.
14. Velkov, M. Behaviour of Large Panel Building during the Romania Earthquake of March 4, 1977. In Proceedings of the IABSE Seminar on Constructions in Seismic Zones, III, Bergamo, Italy, 10–13 May 1978. [CrossRef]
15. Klyachko, M.; Mortchikchin, I.; Nudga, I. *Large Reinforced Concrete Panel Buildings (Series 122, 135 and 1-464c); Housing Report # 55; World Housing Encyclopedia*; Earthquake Engineering Research Institute (EERI) & International Association for Earthquake Engineering (IAEE): Oakland, CA, USA, 2002.
16. Hadjiyski, K.D.; Simeonov, S.M.; Botev, E.A. The May 22, 2012 Mw= 5.6 Pernik Earthquake—Local Effects and Seismic Impact on Sofia City. In Proceedings of the SE-50EEE Conference, Skopje, North Macedonia, 28–31 May 2013; pp. 29–31.
17. Vasilev, G.; Bonev, Z. Earthquake in Pernik, Bulgaria, 22-nd of May, 2012. In *Bauhaus Summer School 2012: Model Validation and Simulation*; Bauhaus-Universität: Weimar, Germany, 2012.
18. Uroš, M.; Šavor Novak, M.; Atalić, J.; Sigmund, Z.; Baniček, M.; Demšić, M.; Hak, S. Post-earthquake damage assessment of buildings—Procedure for conducting building inspections. *Građevinar* **2020**, *72*, 1089–1115. [CrossRef]
19. Atalić, J.; Uroš, M.; Šavor Novak, M.; Demšić, M.; Nastev, M. The Mw5.4 Zagreb (Croatia) Earthquake of 22 March 2020: Impacts and Response. *Bull. Earthq. Eng.* **2021**, *19*, 3461–3489. [CrossRef]
20. Velkov, M.; Ivkovich, M.; Perishich, Z. Experimental and Analytical Investigation of Prefabricated Large Panel Systems to be Constructed in Seismic Regions. In Proceedings of the 8th World Conference on Earthquake Engineering (8WCEE), San Francisco, CA, USA, 20–28 July 1984.
21. Oliva, M.G.; Clough, R.W.; Velkov, M.; Gavrilovic, P. Correlation of Analytical and Experimental Responses of Large-Panel Precast Building Systems. In *Earthquake Engineering Research Center, UCBIEERC-83/20*; University of California: Berkeley, CA, USA, 1988.
22. Brzev, S.; Petrović, M.; Milićević, I. Seismic Behavior of Precast Reinforced Concrete Large Panel Buildings: A Case of Jugomont System. *J. Earthq. Eng.* **2026**, 1–37. [CrossRef]
23. Clough, R.W.; Malhas, F.; Oliva, M.G. Seismic Behavior of Large Panel Precast Concrete Walls: Analysis and Experiment. *PCI J.* **1989**, *34*, 42–66. [CrossRef]
24. Brzev, S.; Zugic, Z.; Guri, M.; Gjuzi, O. Seismic Behaviour of Prefabricated Large Panel Reinforced Concrete Buildings Considering the Effect of Local Soil Conditions. In Proceedings of the 3rd European Conference on Earthquake Engineering & Seismology, Bucharest, Romania, 4–9 September 2022; pp. 919–928.
25. Kollegger, J.P.; Bouwkamp, J.G. *Predictive Dynamic Response of Panel Type Structures Under Earthquakes*; University of California, Earthquake Engineering Research Center: Berkeley, CA, USA, 1980.
26. Schricker, V.; Powell, G.H. *Inelastic Seismic Analysis of Large Panel Buildings*; University of California, Earthquake Engineering Research Center: Berkeley, CA, USA, 1980.
27. Kianoush, M.R.; Elmorsi, M.; Scanlon, A. Response of Large Panel Precast Wall Systems: Analysis and Design. *PCI J.* **1996**, *2*, 1. [CrossRef]
28. Pall, A.S.; Marsh, C.; Fazio, P. Friction Joints for Seismic Control of Large Panel Structures. *PCI J.* **1980**, *25*, 38–61. [CrossRef]

29. Sanchez, J.; Toranzo, L.; Nixon, T. Seismic Performance Evaluation of an Existing Precast Concrete Shear Wall Building. In Proceedings of the 15th World Conference on Earthquake Engineering (15WCEE), Lisbon, Portugal, 24–28 September 2012.
30. Mueller, P. Behavioral Characteristics of Precast Walls. In *Proceedings of the a Workshop on Design of Prefabricated Concrete Buildings for Earthquake Loads*; Applied Technology Council: Berkeley, CA, USA, 1981; pp. 278–308.
31. Becker, J.M.; Llorente, C.; Mueller, P. Seismic Response of Precast Concrete Walls. *Earthq. Engng Struct. Dyn.* **1980**, *8*, 545–564. [CrossRef]
32. Abaev, Z.; Valiev, A.; Kodzaev, M. Large Panel Reinforced Concrete Buildings Inelastic Behavior Modeling Approach for Nonlinear Seismic Analysis. In *Proceedings of the 7th International Conference on Construction, Architecture and Technosphere Safety*; Radionov, A.A., Ulrikh, D.V., Timofeeva, S.S., Alekhin, V.N., Gasiyarov, V.R., Eds.; Lecture Notes in Civil Engineering; Springer Nature: Cham, Switzerland, 2024; Volume 400, pp. 162–174; ISBN 978-3-031-47809-3.
33. Bakrysheva, V.V.; Shahskin, K.G. Methods of Setting Stiffness of Horizontal Joints of Large-Panel Buildings at Soil-Structure Interaction Calculation. In *Smart Geotechnics for Smart Societies*; CRC Press: London, UK, 2023; pp. 1563–1568; ISBN 978-1-003-29912-7.
34. Socarrás Cordoví, Y.C.; Álvarez Deulofeu, E.R.; Vidaud Quintana, I.; Calzadilla Téllez, M.; Pompa Nuñez, R. Seismic Behavior of Large Concrete Panel Prefabricated Structures in Relation to Structural Joints. *Acta Sci. Technol.* **2024**, *46*, e64476. [CrossRef]
35. Jevtic Rundek, R.; Uros, M.; Demsic, M.; Savor Novak, M.; Pilipovic, A.; Koscak, J. Failure Mechanism and Load Bearing Capacity of a Typical Pre-Code Wall Panel System. In Proceedings of the 18th World Conference on Earthquake Engineering (18WCEE), Milan, Italy, 30 June–5 July 2024.
36. Central Technical Construction Archive (AQTN). *Original Archival Drawings and Technical Documentation of Large Panel Buildings*; Central Technical Construction Archive: Tirana, Albania, 1979.
37. State Committee for Civil Construction and Architecture. *VSN 32-77*; Instruction for the Design of Structures of Panel Residential Buildings. Gosgrazhdanstroy: Moscow, Russia, 1978. (In Russian)
38. *SP 335.1325800.2017*; Large-Panel Construction Systems. *Design Rules*; Minstroy of Russia: Moscow, Russia, 2017. (In Russian)
39. Abaev, Z.; Valiev, A.; Kodzaev, M. Methodology of Determination of the Platform Joint of Reinforced Concrete Large-Panel Buildings Stiffnesses. In *Proceedings of the 6th International Conference on Construction, Architecture and Technosphere Safety*; Radionov, A.A., Ulrikh, D.V., Timofeeva, S.S., Alekhin, V.N., Gasiyarov, V.R., Eds.; Lecture Notes in Civil Engineering; Springer International Publishing: Cham, Switzerland, 2023; Volume 308, pp. 277–286; ISBN 978-3-031-21119-5.
40. LIRALAND Group. Large Panel Buildings: Parametric Design of Large Panel Buildings in LIRA-SAPR. Available online: https://www.liraland.com/lira/systems/panel.php (accessed on 20 May 2024).
41. Malakhova, A.; Davletbaeva, D. The Consideration of Compliance of Structural Joints in Calculation of Large Panel Buildings. *E3S Web Conf.* **2019**, *97*, 04010. [CrossRef]
42. Filaj, E. Studim Mbi Parametrat e Përcaktuar Kombëtarë Për Konstruksionet e Çelikut Sipas Eurokodeve. Ph.D. Thesis, Polytechnic University of Tirana, Tirana, Albania, 2017.
43. *EN 1992-1-1:2004*; Eurocode 2—Design of Concrete Structures-Part 1-1: General Rules and Rules for Buildings. European Committee for Standardization (CEN): Brussels, Belgium, 2004.
44. Cardenas, A.E.; Hanson, J.M.; Corley, W.G.; Hognestad, E. Design Provisions for Shear Walls. *ACI J.* **1973**, *70*, 221–230. [CrossRef]
45. Brzev, S.; Pao, J. *Reinforced Concrete Design—A Practical Approach*, 4th ed.; John Pao Publishing: Vancouver, BC, Canada, 2026.
46. *EN 1993-1-1*; Eurocode 3—Design of Steel Structures-Part 1-1: General Rules and Rules for Buildings. European Committee for Standardization (CEN): Brussels, Belgium, 2005.
47. *KTP 10-78, Libri III*; Kushtet Teknike të Projektimit për Konstruksionet prej Çeliku. Shtëpia Botuese "8 Nëntori": Tirana, Albania, 1978.

https://doi.org/10.3390/buildings16173399